An extended Cellular Potts Model analyzing a wound healing assay

An Extended Cellular Potts Model Analyzing a Wound Healing Assay

Marco Scianna[1]

Department of Mathematics, Politecnico di Torino, Corso Duca degli Abruzzi 24, 10129 Torino, Italy

Abstract

A suitable Cellular Potts Model is developed to reproduce and analyze an *in vitro* wound-healing assay. The proposed approach is able both to quantify the invasive capacity of the overall cell population and to evaluate selected determinants of single cell movement (velocity, directional movement, and final displacement). In this respect, the present CPM allows to capture differences and correlations in the migratory behavior of cells initially located at different distances from the wound edge. In the case of an undifferentiated extracellular matrix, the model then predicts that a maximal healing can be obtained by a chemically induced increment of cell elasticity and not by a chemically induced downregulation of intercellular adhesive contacts. Moreover, in the case of two-component substrates (formed by a mesh of collagenous-like threads and by a homogeneous medium), CPM simulations show that both fiber number and cell-fiber adhesiveness influence cell speed and wound closure rate in a biphasic fashion. On the opposite, the topology of the fibrous network affects the healing process by mediating the productive directional cell movement. The paper, also equipped with comments on the computational cost of the CPM algorithm, ends with a throughout discussion of the pertinent experimental and theoretical literature.

Keywords:
cellular Potts model, cell compartmentalization, cell migration, extracellular matrix, invasion front, wound healing assay

[1]E-Mail: `marcosci1@alice.it`

1. Introduction

Cell migration is a fundamental process occurring in a wide range of physio-pathological situations, both in embryogenesis and in adult life. Cells can move *individually* or *collectively*, i.e., as multicellular aggregates. Single cell migration is mainly regulated by cellular and subcellular mechanisms, including actin filaments polymerization [91, 99, 104], focal adhesion point turnovers [65] and proteolytic activity [138, 139]. Mechanotransduction and inside-out signal exchange with the extracellular environment are important as well [126]. Collective migration involves instead multicellular dynamics, mainly coordinated via cell-cell junctions [45, 66, 128]. Functional and phenotypical differentiations of individuals within the same aggregate also occur during multicellular movement [66]. Samples of collective cell migration can be found in morphogenesis, cancer growth and development, and tissue repair after lesions [45].

Coordinated movement of cell populations has been analyzed by a wide range of *in vitro* models (see [3, 53, 63, 64, 67, 113] for relevant examples). In particular, one of the most commonly employed experimental systems is the *in vitro wound healing assay* [11, 13, 15, 41, 84, 101, 128, 141]. It is based on a cell monolayer first grown to confluence and then artificially scraped using a sharp object (such as pipette tip), see Fig. 1. Wounded areas can be created with other procedures as well [44, 92]. The wound healing assay can be considered the laboratory counterpart of an *in vivo* heal of a lesion. The rate of advance of the wound edge, i.e., the quantification of the area recolonized, gives a measure of the migratory capacity of the population of interest. In this respect, this technique is widely used to compare the invasive potential of specific cell lines either in "resting conditions" (in serum-deprived medium, i.e., in low concentration of growth factors and hormones) or in response to i) specific chemical stimulations, ii) modifications of the expression of molecules putatively involved in migratory processes and iii) topological and structural variations of the matrix-like coating substrates. This last aspect is particularly exploited by biomedical sciences, with the aim of producing and testing bioengineered scaffolds which can provide optimal extracellular environments for regrowth and regeneration of tissues, for example skin, peripheral nerves, bones or cartilage (the literature on this topic is very large, the reader can refer for instance to [19, 122, 142] and references therein).

In this article, an experimental wound healing assay is reproduced by a suitable version of the Cellular Potts Model (CPM), a lattice-based Monte

Carlo technique which employs a stochastic energy minimization to display the evolution over time of cell systems [6, 57, 58, 60, 83]. The proposed model integrates a series of previous works that, based on the CPM extensions presented in [116, 117], deal with different aspects of cell migration within selected matrix environments [118, 119, 120]. However, with respect to those papers, the focus here is the analysis of the collective invasive ability of an entire cell population rather than the study of the migratory capacity of single or isolated cells. From this perspective, this article aims at investigating not only the effect on wound recovering of variations in cell and matrix determinants, but also the role played by a spontaneous phenotypical differentiation (i.e., not prescribed *a priori* by the model) occurring between individuals located in specific areas of the cell culture (i.e., at different distances from the wound edge).

The rest of this paper is organized as follows. Section 2 clarifies the assumptions on which the proposed approach is based. As a relevant model feature, each virtual cell is represented as a discrete compartmentalized object (differentiated in nucleus, cytosol and plasma membrane) with individual properties. Different types of substrate, which differ for homogeneity, topology and density of fibrous component are employed as well. Selected numerical results are shown in Section 3. The end of Section 3 focuses on a study of the computational cost of the CPM algorithm. The simulation outcomes are finally discussed in Section 4, where comparisons with proper results from both the experimental and the pertinent computational literature are provided as well.

2. Mathematical Model

In vitro wound healing is simulated using an extended Cellular Potts Model, a grid-based stochastic approach, which describes the evolution of the cell culture in energetic terms and elastic constraints. The simulation domain is a bidimensional lattice (i.e., a regular numerical repeated graph) $\Omega \subset \mathbb{R}^2$, coherently with the planarity of most healing processes. Ω is partitioned by disjoint close sites that, with an abuse of notation, are identified by their center point $\mathbf{x} \in \mathbb{R}^2$. Following, for consistency, the same notation adopted in [116, 117], a neighboring site of $\mathbf{x}$ is here denoted by $\mathbf{x}'$ and its overall neighborhood by $\Omega'_{\mathbf{x}}$, i.e., $\Omega'_{\mathbf{x}} = \{\mathbf{x}' \in \Omega : \mathbf{x}' \text{ is a neighbor of } \mathbf{x}\}$. Each site $\mathbf{x} \in \Omega$ is then labeled by an integer number, $\sigma(\mathbf{x}) \in \mathbb{N}$, which can be interpreted as a degenerate *spin* originally coming from statistical physics

[69, 100]. Subdomains of contiguous sites with identical spin form discrete *standard* objects, which are characterized by an object type, τ. The virtual cells, identified by an integer $\eta = 1, ..., N$ where N is their total number, are here defined as *compartmentalized* objects. They are in fact composed of three subunits which, in turn, are standard CPM objects: the nucleus, a central more or less round cluster of type $\tau = N$, the surrounding cytosol, $\tau = C$, and the plasma membrane (PM), $\tau = M$, which is one-site wide and encloses the entire cell, see Fig. 2. Each subcellular compartment is obviously characterized, as an off-lattice additional attribute, by the cluster id η to identify the cell it belongs to. The nuclear membrane is not explicitly modeled, as it is defined as the interface between the cytosolic compartment and the nuclear region.

Terminological remark. Compartmentalized objects indicate CPM elements (in this case, cells) composed by a set of standard CPM objects which, in turn, indicate simple lattice subdomains sharing the same spin (in this case, cell nuclei, cytosolic regions, and plasma membranes).

The cell population is seeded on a matrix substrate, which is differentiated in a homogeneous medium-like state, $\tau = Q$, and an inhomogeneous collagen-like state, $\tau = F$. The medium-like state simulates a gelatinous substrate, which is composed by a mixture of soluble components (among others, long carbohydrate polymers, and non-proteoglycan polysaccharides) and water solvent. It is assumed to be isotropically distributed throughout the simulation domain, forming no large-scale structures. Instead the collagen-like state represents fixed assemblies of insoluble macromolecules, such as collagens, laminin and elastin, that associate into fibers. Each fiber is here individually modeled by a standard non-compartmentalized CPM object. Distribution and number of fibrous structures will be specified in Sec. 3 and will reproduce different types of matrix substrates typically employed for *in vitro* assays. The inclusion of an explicit two-component extracellular environment is already present in some CPM applications focused on tumor growth [56, 107] and single cell migration [118]. It is a fundamental aspect also of this work because it allows a detailed analysis of the relationship between selected determinants of the matrix substrate (i.e., density and topology) and the healing properties of the cell culture.

Cell dynamics are determined by an energy minimization principle. In more details, the simulated system evolves to iteratively and stochastically reduce its free energy, given by an *hamiltonian* H, whose expression will

be clarified below. The core algorithm is a modified version of the classical Metropolis method for Monte Carlo-Boltzmann thermodynamics [60, 89]. It is particularly suitable to implement the natural exploratory behavior of cells, reproducing their cytoskeletally-driven membrane fluctuations and extensions of pseudopods through repeated probabilistic updates of the site identification spins σ.

Procedurally, in every step t of the algorithm, called Monte Carlo Step (MCS), a lattice site, $\mathbf{x}_{source}$, is selected at random and assigns its spin, $\sigma(\mathbf{x}_{source})$, to one of its unlike neighbors, $\mathbf{x}_{target} \in \Omega'_{\mathbf{x}_{source}}$, also randomly selected. The net energy difference due to the proposed change of domain configuration,

$$\Delta H|_{\sigma(\mathbf{x}_{source})\to\sigma(\mathbf{x}_{target})} = H_{(after\ spin\ copy)} - H_{(before\ spin\ copy)},$$

is then evaluated. The trial spin update is finally accepted with a Boltzmann-like probability function:

$$\begin{aligned} &P(\sigma(\mathbf{x}_{source}) \to \sigma(\mathbf{x}_{target}))(t) = \\ &= \tanh(T_{\sigma(\mathbf{x}_{source})}(t)) \min\left\{e^{-\Delta H|_{\sigma(\mathbf{x}_{source})\to\sigma(\mathbf{x}_{target})}/T_{\sigma(\mathbf{x}_{source})}(t)}, 1\right\}, \end{aligned} \tag{1}$$

where $T_{\sigma(\mathbf{x}_{source})}(t) \in \mathbb{R}^+$ is a Boltzmann temperature which, in this context, measures the agitation rate of moving compartment $\sigma(\mathbf{x}_{source})$. The specific form of (1) is identified so that it is possible to account also for cells with substantially null motility, i.e., for which the probability of moving is negligible even in the presence of favorable energy gradients, as commented in [116]. Specifically, for any cell η and for $\tau(\sigma(\mathbf{x}_{source})) = N$, $T_{\sigma(\mathbf{x}_{source})}(t) = T_N$ is a constant low value mimicking the passive motion of the nucleus, which is dragged by the surrounding cytosolic region via actin filaments and microtubules (see [115] for a specific mechanical explanation). For any cell η and for $\tau(\sigma(\mathbf{x}_{source})) = C, M$, $T_{\sigma(\mathbf{x}_{source})}(t)$ gives a measure of the cell intrinsic motility, representing the agitation of the cell cytoskeleton and the frequency of PM ruffles, respectively. Both are assumed to be chemically stimulated in a dose-dependent manner:

$$T_{\sigma(\mathbf{x}_{source}):\tau(\sigma)=C,M}(t) = T_0 \left[\frac{c^\eta(t)}{c_0^\eta + h\,(c^\eta(t) - c_0^\eta)}\right]. \tag{2}$$

In (2), for any MCS t, $c^\eta(t) = \sum_{\mathbf{x}\in\eta} c(\mathbf{x}, t)$ gives the total amount of chemical within η, the cell to which the moving compartment $\sigma(\mathbf{x}_{source})$ belongs to.

In fact, $c(\mathbf{x}, t)$ indicates the present concentration of the substance (see Eq. (6) below). Instead $c_0^\eta = \sum_{\mathbf{x}\in\eta} c_0$ is the basal level of the chemical, as c_0 indicates the initial intracellular concentration, a characteristic of the cell line of interest. In this respect, T_0 corresponds to the basal motility of the cells (assumed to be substantially low), while T_0/h is the asymptotic motility for a saturating concentration of the chemical. For the sake of clarity, it is useful to recall that hereafter the simplified notation $\mathbf{x} \in \eta$ is used to identify a site $\mathbf{x}$ belonging to the compartmentalized cell η, even if the exact expression would be $\mathbf{x} \in \sigma(\mathbf{x}) \subset \eta$.

During wound invasion, cells can only temporarily occupy, but not permanently modify, the position or the original content of a matrix site. For example, if a cell moves from a site previously occupied by a fiber, the site is restored to its previous collagenous-like state. In this respect, the virtual substrate is assumed passive and conserved, as matrix digestion and/or deposition are neglected.

For any given MCS t, the system free energy, whose minimization, as seen, drives the evolution of the cell culture, is:

$$H(t) = H_{shape}(t) + H_{adhesion}(t). \tag{3}$$

H_{shape} models the geometrical attributes of all cell subunits. They are written as non-dimensional relative deformations in the following quadratic form:

$$\begin{aligned} &H_{shape}(t) = H_{volume}(t) + H_{surface}(t) = \\ &= \sum_{\eta,\sigma} \left[\kappa_{\eta,\sigma}(t) \left(\frac{v_{\eta,\sigma}(t) - V_{\tau(\sigma)}}{v_{\eta,\sigma}(t)} \right)^2 + \nu_{\eta,\sigma}(t) \left(\frac{s_{\eta,\sigma}(t) - S_{\tau(\sigma)}}{s_{\eta,\sigma}(t)} \right)^2 \right]. \end{aligned} \tag{4}$$

$v_{\eta,\sigma}(t)$ ($s_{\eta,\sigma}(t)$, respectively) is the actual volume (surface, respectively) of compartment σ of cell η, while $V_{\tau(\sigma)}$ ($S_{\tau(\sigma)}$, respectively) is the corresponding initial measure. The specific formulation of (4) allows to have finite energetic contributions, as well as a blow up in the case of $v_{\eta,\sigma}(t), s_{\eta,\sigma}(t) \to 0$ (see again [116]). $\kappa_{\eta,\sigma}(t)$, $\nu_{\eta,\sigma}(t) \in \mathbb{R}^+$ are mechanical moduli in units of energy. In particular, $\kappa_{\eta,\sigma}(t)$ refer to volume changes of subcellular units, while $\nu_{\eta,\sigma}(t)$ relate to their elasticity, the ease with which they are allowed to remodel. Assuming that cells do not significantly grow during the healing process (here nutrients are not taken into account), the fluctuations of their volumes are kept negligible with high constant values of $\kappa_{\eta,\sigma} = \kappa$, for any couple η, σ. Moreover, cell nuclei typically have a low compressibility: therefore, for all η

and for $\sigma : \tau(\sigma) = N$, $\nu_{\eta,\sigma} = \nu$ is another high constant quantity. In a first approximation, the chemical substance is not assumed to induce a dramatic reorganizations of cell cytoskeleton and plasma membrane. In this respect, for any cell η, it is reasonable to set $\nu_{\eta,\sigma} = \nu$ also for $\tau(\sigma) = C, M$. This way cells are forced to remain in the initial round morphology. However, selected simulations in Sec. 3 will study how the invasive behavior of the cell culture is affected by the introduction of a chemically induced remodeling of cell morphology.

$H_{adhesion}$ is the general extension of Steinberg's Differential Adhesion Hypothesis (DAH) [60, 123, 124]. In particular, it is differentiated in the contributions due to either the generalized contact between subunits belonging to the same cell, or to the effective adhesion between membranes of different cells, see Fig. 2 (and refer to[116] for details):

$$\begin{aligned} H_{adhesion}(t) &= H^{int}_{adhesion}(t) + H^{ext}_{adhesion}(t) = \\ &= \sum_{\mathbf{x}\in\Omega,\mathbf{x}'\in\Omega'_{\mathbf{x}}} \left[J^{int}_{\tau(\sigma(\mathbf{x})),\tau(\sigma(\mathbf{x}'))}\delta_{\eta(\mathbf{x}),\eta(\mathbf{x}')}(t)(1-\delta_{\sigma(\mathbf{x}),\sigma(\mathbf{x}')}(t))\right] + \\ &+ \sum_{\mathbf{x}\in\Omega,\mathbf{x}'\in\Omega'_{\mathbf{x}}} \left[J^{ext}_{\tau(\sigma(\mathbf{x})),\tau(\sigma(\mathbf{x}'))}(1-\delta_{\eta(\mathbf{x}),\eta(\mathbf{x}')}(t))\right], \end{aligned} \tag{5}$$

where $\mathbf{x}$, $\mathbf{x}'$ represent two neighboring lattice sites, $\delta_{x,y} = \{1, x = y; 0, x \neq y\}$ is the Kronecher delta, and the Js are symmetric binding energies per unit of area. In particular, $J^{int}_{\tau(\sigma(\mathbf{x})),\tau(\sigma(\mathbf{x}'))}$, where $(\tau(\sigma(\mathbf{x})), \tau(\sigma(\mathbf{x}'))) = (C, N)$ or (C, M), are constant high tensions which prevent cells from fragmenting (unrealistic contacts between the nucleus and the PM within same individual are not accounted for). $J^{ext}_{\tau(\sigma(\mathbf{x})),\tau(\sigma(\mathbf{x}'))}$, for $(\tau(\sigma(\mathbf{x})), \tau(\sigma(\mathbf{x}'))) = (M, M)$, represents instead the local adhesive strength between the membranes of two different cells. It is indeed a measure of the local quantity of active exposed cadherins. Finally, $J^{ext}_{\tau(\sigma(\mathbf{x})),\tau(\sigma(\mathbf{x}'))}$, for $(\tau(\sigma(\mathbf{x})), \tau(\sigma(\mathbf{x}'))) = (M, Q)$ or (M, F), evaluate the adhesive interactions of the cells with the gelatinous medium and the collagen-like fibers, respectively. In this respect, $J^{ext}_{M,Q}$ and $J^{ext}_{M,F}$ are a measure of the affinity between cell surface adhesion complexes (i.e., sugar-binding receptors or integrins) to either non-solid (i.e., glycosaminoglycans in medium) or solid (i.e., fibrillar collagen) extracellular ligands, respectively [112]. As given in Table 1, and explained in the section on Material and Methods, external and internal contact energies are set constant in time and homogeneous in space. However, a set of simulations will dissect the role in the healing process of an agent-induced downregulation of

cell-cell adhesive interactions, which is observed in a wide range of cell lines stimulated by several substances.

At any given MCS t, the spatial profile of the chemical, $c(\mathbf{x}, t)$, satisfies the following reaction-diffusion (RD) equation:

$$\frac{\partial c(\mathbf{x},t)}{\partial t} = \underbrace{D\nabla^2 c(\mathbf{x},t)}_{diffusion} - \underbrace{\lambda c(\mathbf{x},t)}_{degradation} - \underbrace{\min\{\beta, kc(\mathbf{x},t)\}\delta_{\tau(\sigma(\mathbf{x})),\{N,C,M\}}}_{consumption} + \underbrace{S(t)}_{addition}, \tag{6}$$

where D and λ are the characteristic diffusion coefficient and degradation rate of the chemical substance, respectively. Both are assumed constant and homogeneous throughout the simulated domain. $S(t)$ describes the addition of the chemical at a constant saturating rate s_c outside the cells. The third term at the right-hand-side of Eq. (6) models instead the amount of chemical molecules absorbed by the cells, i.e., it is not null if $\tau(\sigma(\mathbf{x})) = N, C$, or M. It follows a piecewise-linear approximation of a Michaelis-Menten law. This simplification is realistic since the capacity of a cell to absorb chemicals typically saturates to a limit, which is established both by the density of membrane-bound receptors and by the rate at which the chemical substance can be internalized and the receptors recycled, see also [8, 79]. In particular, $\lambda \ll k$, as the chemical natural decay is assumed to be negligible compared to the cell uptake.

3. Results

3.1. Algorithm and simulation details

The simulation domain Ω is a lattice of 350×500 sites. The characteristic length of each site is scaled to 2 μm: therefore Ω represents a section of a well of size 0.7 mm $\times$ 1 mm. As explained in the section on Materials and Methods, an empirical calibration between numerical and experimental results allows to find out the correspondence between 1 MCS and 2 seconds. The boundary conditions of domain Ω are zero flux at the left side (i.e., at $x = 0$) and periodic at the others (i.e., at $x = 350$, $y = 0$, and $y = 500$). The no flux assumption at $x = 0$ is appropriate as cell populations in wound healing assays grow to confluence and therefore there is no space for cells to move in that direction of the domain. The periodic boundary conditions at the top and the bottom of the lattice are also reasonable since the model deals with a section of a much larger well. The periodic conditions at $x = 350$ are instead arbitrarily set to reduce boundary effects.

In all simulation setting, the stimulation with the chemical substance is modeled by imposing in Eq. (6) $S(t) = s_c$ for $t \in [165, 195]$ min (i.e., for $t \in [4950, 5850]$ MCS). This condition implements a constant addition of a saturating (i.e., very high) level of chemical for 30 minutes after 2 hours and 45 minutes from wound scraping.

The algorithm underlying the proposed simulations combines a numerical scheme for solving the reaction-diffusion equation of the chemical substance with an iterative procedure for implementing the Metropolis Monte Carlo method characteristic of CPM approaches. In more details, the former manages the evolution of the chemical concentration while the latter updates cell positions. This resulting conceptual algorithm, schematized in Fig. 3 (left panel), can be described as follows:

1. *Initialization.*

   - The initial configuration of all simulations consists of a mass of compartmentalized cells (the initial/target dimensions of the three subcellular units are given in Table 1) placed at the 175 site $\times$ 500 site (i.e., 0.35 mm $\times$ 1 mm) left part of the domain (see the right panel of Fig. 3). The area deprived of cells reproduces the experimental wound. The width of the scratch (i.e., 175 site $\approx$ 0.35 mm) is lower than in most experimental cases to avoid cell overlapping and to supply to the absence of mitosis. The intracellular basal concentration of the chemical, c_0, is assumed to be spatially homogeneous, while the initial extracellular level of the substance is zero. All cells are assumed to have the very same basal properties (i.e., intrinsic motility, adhesiveness, elasticity). The type of matrix will change for each set of simulations;
   - The cell culture is then annealed for 100 Monte Carlo sweeps according to the following rule:

$$P(\sigma(\mathbf{x}_{source}) \to \sigma(\mathbf{x}_{target})) = \\ = \begin{cases} 0 & \text{if} \quad \Delta H|_{\sigma(\mathbf{x}_{source})\to\sigma(\mathbf{x}_{target})} > 0\,; \\ \dfrac{1}{2} & \text{if} \quad \Delta H|_{\sigma(\mathbf{x}_{source})\to\sigma(\mathbf{x}_{target})} = 0\,; \\ 1 & \text{if} \quad \Delta H|_{\sigma(\mathbf{x}_{source})\to\sigma(\mathbf{x}_{target})} < 0\,, \end{cases} \tag{7}$$

     The annealing procedure prevents matrix-like spins from intermixing with cell spins, therefore allowing the formation of natural-looking and coherent cell boundaries. It also allows to have stable

contacts between the subcompartments forming each individual cell.

2. *Advance in time.*

   - The discrete CPM evolves through a MCS, following the rules given in Eq. (1);
   - The continuous equation of the chemical is rederived, according the new cell configuration, and solved, using a finite element scheme on a grid with the same spatial resolution as Ω, characterized by 10 diffusion time steps per MCS (this temporal step is sufficiently small to guarantee numerical stability);
   - The properties of all cells (i.e., motility and, eventually, elasticity and adhesiveness) are updated, given their new biochemical state (i.e., the new amount of internalized chemical molecules);
   - The hamiltonian functional in Eq. (2) is recalculated, and the system is ready to evolve again.

3. *Final time.* To model a pure migration assay, the overall observation period is set equal to 21600 MCS, which correspond to nearly 12 hours, for all simulation settings. This choice assures a sufficient distance from critical events, such as culture splitting and cell cycle synchronization.

3.2. Wound healing in the case of a homogeneous collagen-free matrix

The first sets of simulations analyze the healing capacity of the cell population in an isotropic collagen-free matrix.

Chemically stimulated vs. non-stimulated healing process. Without chemical stimuli (i.e., obtained by setting $S(t) = 0$ for any t in Eq. (6)), the virtual culture is characterized by a poor invasive phenotype, as $D(t = 12\text{ h}) \approx 10\%$ (see Fig. 4). This phenomenology is the consequence of the low basal cell motility, given by T_0 in Eq. (2), which is not able to overcome intercellular adhesive contacts thereby not allowing single individuals to spread in the wound area. In this respect, the slight expansion of the population edge is only due to cell body relaxation. On the other hand, upon chemical stimulation, the cell culture is observed to have a significant invasive ability, as the population edge (now composed by a front of dispersed individuals) is strongly biased towards the gap ($D(t = 12\text{ h}) \approx 40\%$, see Fig. 5).

Differences and correlations in the migratory behavior of groups of cells located at different distances from the edge of the wound can now be analyzed. In particular, external, middle and internal cell subpopulations can be distinguished (see the graphically delimited regions in Fig. 5). For consistency, the correspondence between each subpopulation and the specific representative color, i.e., red-external, blue-middle, green-internal, is maintained hereafter in all graphs. As quantitatively evaluated in Fig. 6, cells placed close to the edge of the scratch are characterized by a high short-range motility. In particular, such external individuals typically move according to angles that moderately cluster around the expected direction, i.e., towards the middle of the wound, showing indeed a quite relevant value of linearity ($L \approx 0.6$). Cells located in an intermediate position have instead decreased net displacement and linearity. Finally, cells far away from the front of the culture feature an almost negligible movement. A further confirmation of the different dynamics of the three subpopulations is given by the modulus of their instantaneous velocity, plotted in Fig. 6(C): external cells move significantly faster than middle cells, and the velocity is almost negligible for internal individuals. It is indeed possible to state that the migratory capability of a cell decreases when its initial distance from the edge of the wound increases. The rationale of such a phenotypic differentiation is two-fold: on one hand, cells placed in the more external regions of the culture have access to a greater amount of chemical factor (which is almost completely uptaken before diffusing in the internal areas of the mass), thereby enhancing their motility. On the other hand, cells located far enough from the wound edge experience higher cell densities and therefore are subjected to the so-called *contact inhibition of cell locomotion*. This phenomenon, first proposed by Abercrombie [1] and widely observed in wound healing models of epithelial cell lines [143] and fibroblast cultures [132], consists in the fact that cells within closely packed aggregates do not move since they are strictly held by surrounding individuals (via intercellular adhesiveness). Finally, from Fig. 6(C), it is possible to observe that, for any cell η, $|\mathbf{v}(t)|$ is an increasing function of time. This characteristic of the cell speed (obviously more evident for external individuals) depends on the fact that: i) the intracellular amount of chemical $c^{\eta}(t)$ raises up and ii) as the culture expansion advances, cells are surrounded by more open space to spread across.

In order to validate the proposed theoretical approach, the results obtained from the Monte Carlo simulations are now compared with the outcomes of selected wound healing assays performed by the group of Prof. Fu-

naro and E. Ortolan at the Laboratory of Immunogenetics of the University of Turin Medical School. In particular, their experiments focus on the healing behavior of cultures of ovarian cancer cells (specifically, NIH:OVCAR-3) stimulated or not with CD157. CD157 is a glycosylphosphatidylinositol-anchored glycoprotein encoded by a member of the nicotinamide adenine dinucleotide glycohydrolase (NADase)/ADP-ribosyl cyclase gene family [43, 70, 95]. It is involved in several cellular functions, including regulation of humoral immune response and of leukocyte trafficking [51, 52, 68]. CD157 also affects the interactions between the mesothelium and ovarian tumor cells, ultimately controlling ovarian cancer dissemination and peritoneal invasion [94]. As summarized in Fig. 7, the experimental cell cultures behave similarly to the virtual cell populations both in the non-stimulated condition (MOCK) and after CD157 treatment. In more details, a minimal advance of cell population edges is observed without CD157 transfection. On the opposite, significant wound invasion is observed upon chemical stimulation. To further compare *in silico* and *in vitro* outcomes, initial and final position of some representative experimental cells, initially located at different distances from the borders of the scratch, are tracked and the linearity of their migration is computed. As it is possible to observe in the corresponding panels of Fig. 7, the resulting migratory determinants are consistent with those measured for the corresponding subpopulations of virtual cells.

Terminological remark. Hereafter in the paper, the simulation setting presented in Figs. 5 and 6 will be indicated and recalled as the "reference case".

Chemically induced decrease of intercellular adhesiveness. A number of *in vitro* experiments highlights that a variety of chemicals is able to stimulate cell motility by downregulating cadherin expression and/or activity, i.e., by disrupting cell-cell contact interactions. For example, the hepatocyte growth factor/scatter factor (HGF/SF) causes a loss in E-cadherin signaling in both normal and neoplastic epithelial cells, which consequently feature a dispersed/scattered phenotype [32, 34, 137]. These considerations prompt to investigate the effect on the invasive behavior of the cell population of a chemically induced decrement in cell-cell adhesiveness. In this respect, a plausible constitutive law for the intercellular adhesiveness reads:

$$J^{ext}_{\tau(\sigma(\mathbf{x})),\tau(\sigma(\mathbf{x}')):(\tau(\sigma(\mathbf{x})),\tau(\sigma(\mathbf{x}')))=(M,M)}(t) = J^{ext}_{M,M}\left[\frac{c(\mathbf{x},t)c(\mathbf{x}',t)}{(c_0)^2}\right], \qquad (8)$$

where $c(\mathbf{x},t)$ and $c(\mathbf{x}',t)$ are present intracellular concentrations of the chem-

ical and c_0 the basal value. As explained in the previous section, $J^{ext}_{M,M}$ is the typical adhesive force of resting cells. Notice that relation (8) allows to account for time and space variations (i.e., inhomogeneities along the plasma membrane) of cell-cell adhesiveness. As represented in Fig. 8, the resulting culture invasion of the gap is somewhat quicker but not depth as one could expect. It is in fact possible to observe a dramatic expansion of the cell population during the 3 hours after the chemical stimulation, followed by a stabilization of the wound closure rate. In this respect, the final percentage of invasion is quite similar to the reference case. The observed healing behavior can be explained with the following considerations. The chemical stimulation immediately downregulates adhesive interactions between external cells, which therefore are allowed to quickly spread away from the rest of the mass. Also middle and internal cells undergo a progressive repulsion, with the consequent formation of little islands of free substrate within the culture. Such areas deprived of cells are then filled again by surrounding shedding individuals, thereby do not bias the overall invasion. By analyzing the behavior of the different subpopulations, it is possible to observe that i) the velocity of external cells increases significantly in the aforesaid 3-hours-time-lapse, before stabilizing at the reference value; ii) both internal and middle individuals move faster than in the reference case (this is due to the fact that they dissociate and therefore are longer subjected to the above-mentioned contact inhibition of motility, see Fig. 8(E)); iii) cell average linearity and net final displacement remain however comparable to the reference case, as shown in Fig. 8(C-D). From these results, it is possible to conclude that a chemically induced alteration in cell-cell adhesiveness has, at least in the proposed CPM simulations, a relatively subtle effect on the effective healing capability of a cell population. It in fact affects only the wound closure rate in the initial phases. As a counter proof, a non-stimulated cell population features a negligible healing with the observation period even with a very low value of cell-cell adhesiveness (not shown).

Chemically induced enhancement of cell elasticity. The relation between the healing activity of the population and a chemical-dependent enhancement of cell elasticity is now investigated. In particular, for any cell η, the following constitutive relation is imposed:

$$\nu_{\eta,\sigma:\tau(\sigma)=C,M}(t) = \nu \ \exp\left(-\left[\frac{c^{\eta}(t)}{c_0^{\eta}} - 1\right]\right), \tag{9}$$

where $c^{\eta}(t)$ and c_0^{η} are defined as in Eq. (2) and ν is, as seen, the intrinsic

cell resistance to compression. Relation (9) models the activity of chemical substances that, in a dose-dependent manner, either directly facilitate acto-myosin interactions (such as calcium ions [12]) or activate downstream pathways resulting in actin filaments polarization (for example VEGF isoforms [36, 134]). The consequence of the new model hypothesis is an almost complete closure of the wound within the observation period (i.e., $D(t = 12\text{ h}) \approx 90\%$, see Fig. 9(A-B)). The increased invasive capacity of the population is mainly due to the fact that external cells are able to migrate significantly far across the wound area. In this respect, their movement is characterized by an increment both in the speed value and, more relevantly, in the linearity (i.e., in the directional component), as shown in Fig. 9(C-E). This phenomenology is due to the fact that cells at the front of the culture have sufficient open environs to expand and, stimulated by the availability of chemical factor, organize in a motile elongated phenotype. Such a morphological transition allows them to maintain over time the direction of motion defined by their geometry (*persistent migration*) and therefore to go on traversing the lattice more readily. In turn, this is the reason why the wound closure rate does not stabilize around a threshold value. On the contrary, middle and internal cells, maintaining strong adhesive interactions, are not able to efficiently remodel. As a consequence, they are not observed to have marked changes in velocity, linearity and final displacement distributions w.r.t. the reference setting.

3.3. Wound healing in the case of two-component inhomogeneous matrices

The next simulation settings analyze the healing of the chemically stimulated population in the case of two-component substrates. In particular, the length of single collagenous fibers is set equal to 6 lattice sites ($\approx 12\ \mu$m), accordingly to their typical dimensions in *in vitro* assays [14, 103, 105]. Moreover, although the width of experimental threads generally ranges between 100 nm and 1 μm, they are here accorded the measure of a single site (which the minimum permitted by the grid resolution). It is useful to recall that the hierarchy $J_{M,F} = J_{M,M} < J_{M,Q}$ is assumed and that both cell elasticity and cell-cell adhesiveness are constant values as in the reference case.

In the first set of realizations, an isotropic, moderately dense matrix is formed by a mesh of 1600 collagen threads, equally distributed along each x and y-direction. Because the fibers are randomly arranged, they can overlap: however, the overlap sites are treated identically to non-overlap sites. In these conditions, the cell population displays an evidently increased migratory and

invasive phenotype, as the wound is completely recovered within 9 h, see Fig. 10(B). In particular, the fibrous structure of the matrix does not influence the directional component of cell movement but strongly enhances cell velocity and final displacement, as represented in Fig. 10(C-E). This phenomenology, which is observed for all cell subpopulations but more evident for external individuals, is due to the fact that cells take advantage of the presence of fibrous bundles for traction and further movement. In other words, they use collagenous-sites as "handholds" for deeply invading the gap.

Variation of cell-fiber adhesiveness. These results suggest to investigate the effect of variations in the cell-fiber adhesive strength, given by $J^{ext}_{M,F}$, on the invasive process of the culture. As reproduced in Fig. 11, the resulting population healings can be sorted into three regimes: at high values ($J^{ext}_{M,F} > 6.5$, i.e., the computational counterpart of either an alteration of the relative glycoprotein in the the matrix or of a stimulation with an agent that down-regulates the expression or the activity of integrin molecules) the invasion is discouraged. The cell mass remains in fact relatively compact, with few external cells wade just outside of the front and intermingle with collagenous threads. At moderate values of $J^{ext}_{M,F}$ the invasive capability of the culture increases, since cells are prompted to immediately and efficiently invade along the fibrous network due to an optimal energetic balance between attachment and detachment mechanisms. In particular, the wound is completely invaded within the observation period for $J_{M,F} = 3.5, 4, 4.5$: however, the time characteristic of the process is slightly different, being approximately 9 hours and half, 8 hours, and 9 hours, respectively. Finally, below a certain threshold ($J^{ext}_{M,F} < 3$, which mimics a higher integrin engagement), cells cluster along the nearest fibers and do not further migrate. Given the high difference between $J^{ext}_{M,F}$ and the other adhesive strength ($J^{ext}_{M,M}$ and $J^{ext}_{M,Q}$), the individuals in fact immediately minimize their energy by maximizing collagen contacts. Therefore they have no energetic benefits with further extensions and invasion.

Variation of fiber number. The effect of varying the density of the fibrous component of the substrate is then considered. In this respect, the cell population is planted on lattices with an increasing number of isotropic (i.e., equally distributed along each x and y-axis) fibers, from a low-density mesh to a very high-density scaffold, see Fig. 12(A). As represented in Fig. 12(B), at a number of threads < 250, the lattice is unsaturated and not percolated, and the culture development bears much similarity to the case of a

collagen-free environment (see the reference setting for comparison), as only few external cells interact with collagen-like sites, as represented in the corresponding representative panel in Fig. 14. At low fiber density cells are in fact unable to find sufficient collagen-like sites to attach and use for displacement. At moderate amounts of threads (250, 3000), the invasive capacity of the culture increases with the number of the fibers. The cells (also those in the middle of the mass) find in fact an increasing number of locally available threads to adhere and follow for their migration. Finally, at higher investigated fiber numbers, the healing of the cell population substantially decreases again. An overabundance of fibers causes in fact cells to loose their preference towards collagen contacts, preventing their detachment and further spreading. In particular, when the matrix is formed by a continuous carpet of threads (>20000), the migratory capacity of the culture clearly resembles again that observed in the case of the undifferentiated gelatinous substrate, see Fig. 14(B). Interestingly, the above-described biphasic phenomenology is mediated by a corresponding variation in the instantaneous velocity of cells, whereas the directional component of their movement remains almost unaltered for all the proposed substrates, see panels (C) and (D) of Fig. 12.

Variation of fiber alignment. Finally the development of the cell population in the case of anisotropic matrices is analyzed, see Fig. 13. In particular, substrates formed by 1600 aligned threads disposed with increasing angles ϕ with respect to the x-axis are employed. The maximal invasion is found in the case of $\phi = 0$, i.e., when the fibers are aligned along the horizontal direction, as the wound is completely filled in 6 h, see Fig. 13(B). In particular, external and middle cells are seen to orient alongside collagenous components, which behave as a directional contact-guidance, thereby facilitating cell productive motion towards the center of the lesion, as detailed in Fig. 14(C). Increments in ϕ results in decrements in the healing capability of the culture. Finally, for $\phi = 90°$ (i.e, all threads are disposed along the y-direction) wound invasion is substantially low. In this case, cells tend in fact to cluster around the nearest matrix fibers, whose distribution discourages a further migration towards the scratch, eventually inhibiting the overall invasion, see Fig. 14(D). The variation of the fiber distribution has a clear influence on the linearity characterizing cell migration, while cell mean velocity remains almost constant, as represented in Fig. 13(C-D).

3.4. Analysis of the algorithm performance

As widely known, one of the main drawbacks of CPM implementations is that the underlying algorithm is computationally very expensive, mainly because of the low acceptance probabilities of spin update occurring during each MCS (for a detailed dissertation of this issue the reader is referred to [6, 24]). In this respect, the different sets of simulations presented in this work are now analyzed from a numerical viewpoint. In particular, Fig. 15 shows the running time needed to reach the final observation time (21600 MCS) in selected representative settings: in particular, the so-called "reference case" is, as seen, the one presented in Figs. 5 and 6 while the "two-component matrix case" is the one presented in Fig. 10. First, it can be observed that in the reference case the rate between running time and MCS is approximatively 1/5.4. The implementation of chemical-dependent cell properties results instead in a two-fold increment of running time. In particular, the slight difference between the two values is due to the fact that the elasticity is a global cell parameter, which therefore requires for each MCS the evaluation of the total intracellular amount of chemical, whereas the adhesive strength requires only to monitor local concentrations of the molecular substance. The realizations dealing with two-component matrices (regardless of number and topology of fibers) are instead characterized by almost the same running time as the reference simulation. This is due to the fact that the collagenous components of the matrix are fixed and therefore negligible from a computational viewpoint. Finally, the last value of the plot refers to a simulation of a wound healing assay in the reference setting which employs uncompartmentalized cells (i.e., cells represented by standard CPM objects, thereby without the differentiation in nucleus, cytoplasm and membrane). It is interesting to notice that the running time significantly decreases. The underlying reason is that internal cell compartments are treated by the algorithm as independent CPM objects: therefore, even if the number of cells is the same in the two cases, the number of computational objects varies (i.e., the rate between cells and subunits is 1/3). For the sake of completeness, it is however possible to hypothesize that a population of uncompartmentalized cells wound require less time to invade a wound than a population composed of compartmentalized individuals (in comparable settings). In fact, uncompartmentalized cells would not have to push across the matrix their stiff and less motile nuclear cluster during motion.

4. Discussion

In this work, a simple and intuitive version of the Cellular Potts Model has been proposed to reproduce an *in vitro* wound healing assay, which is one of the most widespread experimental models used to assess the collective and coordinated movement of a multicellular population [11, 13, 15, 41, 44, 84, 92, 101, 128, 141]. In particular, wound healing experiments quantify the capacity of a cell monolayer to invade a scratch in different biological conditions. In this respect, relevant measures are the percentage of the recolonized area and the time needed by the culture to completely repair the wound.

As a distinct model feature, each cell has been represented by a compartmentalized element (i.e., explicitly composed of nucleus, cytosol and plasma membrane), characterized by its own properties (i.e., motility, elasticity and adhesiveness). Variations in structural properties of the matrix substrate have been employed as well, with particular emphasis on density and topology of the fibrous component. The presented approach has been able to describe the invasive behavior of the whole cell population and to evaluate selected migratory determinants (instantaneous velocity, linearity and distribution of the final displacement) of single component individuals. The healing capability of the cell culture has been indeed assessed as the sum of coordinated individual dynamics. In particular, it has been possible to detect the existence of well defined cell subpopulations (namely external, middle, and internal), located at increasing distances from the wound edge and characterized by distinct motility phenotypes. In this respect, simulation outcomes have provided the fact that the healing behavior the population is mainly dictated by the invasive dynamics of the external cells. Intermediate cells have been in fact observed to have a reduced migratory capacity, which is almost negligible for internal individuals. These results have been confirmed, at least in the case of a homogenous gelatinous substrate, by a proper comparison with wound healing experiments performed by the group of Funaro and Ortolan on ovarian cancer cells, treated or not with CD157.

The role played by the more external cells in wound closure processes has been clearly identified in the experimental literature and commonly denoted as *lamellipodia crawling* [44, 84, 109]. This mechanisms relies in fact in the active spreading and migration of individual cells located near the wound edge, which is regulated by specific intercellular biochemical signaling typically activated by mechanical injuries of cell monolayers (i.e., a scratch done by a pipette tip [72, 73, 92, 141]). It has been argued that, in some cases, an

availability of free space is sufficient to initiate external cell migration even in the absence of a mechanical injury [13, 92, 101]. For the sake of completeness, it is useful to mention that a second mechanism of cell movement observed in round wound healing processes is the so-called *purse string*. It consists in a marginal actomyosin cable development along the wound edge, so that wound closure proceeds with contraction of the actin belt [11, 84]. Closure of small wounds in cultures of intestinal epithelial cells can involve the formation of both lamellipodia and purse-string structures as well [11].

The cell phenotypic differentiation captured in the presented CPM is validated by a series of experimental works focused on Madin-Darby canine kidney (MDCK) cells. For instance, in [92], the distance travelled by cells during healing has been observed to be inversely proportional to their initial distance from the edge of the wound (being almost negligible for individuals located far enough from the wound front, consistently with the case of the internal cells of the proposed CPM approach). The authors have found the rationale of this behavior in the specific spatiotemporal pattern of MAPK phosphorylation waves. Such signaling pathways, initiated as a consequence of a mechanical injury of the monolayer, propagate in fact from the edge of the culture to the rest of the mass up to a characteristic distance (nearly 500 μm). Further, these dynamics have not been observed in uninjured cell sheets (the MAPK cascade is no longer activated) or in injured cell sheets treated with MAPK inhibitor. In [41, 42], the authors have provided the fact that a fundamental role in wound closure, at least in MDCK epithelial cell monolayers, is played by cells located several rows behind the wound margin (i.e., which correspond to so-called middle subpopulation of this work). Such submarginal cells have been in fact observed to be able to autonomously initiate migration (by sensing a lowered resistance to movement in one direction or by some chemical or electrical signaling mechanisms) and generate active forces, thereby pushing the more external cells to close the wound. In other words, cells behind the margin are able to actively crawl and coordinately move towards the wound area instead of just passively moving when cells at the margin pull on them. The proposed CPM does not distinguish between active and passive intercellular forces and interactions. It is however possible to speculate that also the virtual middle cells do not move as a consequence of dragging forces exerted via adhesion by external individuals. In accordance with the experimental works, they in fact actively wander in their open proximity. However, as seen more clearly in the case of a chemically induced downregolation of intercellular adhesiveness, the crawling of

middle individuals does not significantly bias the overall healing potential of the population which, as seen, remains mainly determined by the dynamics of cells located near the wound edge.

Specific simulation settings have then demonstrated that, in the case of a homogeneous substrate, the maximal invasiveness of the virtual culture can be obtained with a chemically induced cell remodeling capability and not with a downregulation in the cell-cell adhesiveness, as one could expected.

Cell-cell adhesion has been provided to be an important factor in corneal epithelial wound healing [128]. In particular, the authors have speculated therein that coordinated cell-cell de-adhesion and re-adhesion cycles are required for an optimal recover of the lesion. In fact, too tight intercellular contacts inhibit a sufficient recolonization of the damaged area. The influence in single and collective cell migration of decrements in intercellular adhesiveness has been dissected in details in the case of tumor invasion as well. For instance, a number of experimental studies has recently demonstrated that downregulation of cadherin molecules is implicated in a variety of metastatic cancers [22, 23, 25, 127, 136]. Further, glioma cell lines with low N-cadherin expressions have been observed to aggressively invade matrix gels (whereas the same populations with a high N-cadherin activity have been shown to grow slower and to expand less significantly in the host tissues) [63]. However, it is useful to notice that all these results are in contrast with the outcomes of the proposed model, which instead has predicted that a chemically induced cell-cell detachment does not significantly enhance cell invasion. The rationale of this discrepancy is probably that, in "real" cancer cells, the disruption of intercellular adhesive contacts concomitantly activates a series of intracellular programs (for example, the proteolytic regulatory machinery) that further increase the aggressiveness and metastatic potential of scattered malignant individuals. An aspect that is not included in the presented model.

Cell spreading and shape reorganization have been previously analyzed in several experimental wound healing models. For instance, both the abovementioned wound closure mechanisms (i.e., lamellipodia crawling and purse string) significantly involve cytoskeletal dynamics. In [15, 84], a circumferential ring of actin bundles has been shown to mediate the cell contractile response that draws the wounded edges of embryonic chick wing bud together. In [85], the authors have instead speculated on the fact that, in epithelial cell sheets of adult organisms, active protrusion of filopodia and PM ruffling can be observed in the cells located near the edge of the wound. Consistently, the first phase of a corneal epithelial wound healing consists of

a sheet-like movement, during which cells at the leading front of the monolayer spread over a wide area by extending fan-shaped lamellipodia, as described in [128] and references therein. This is exactly what happens in the proposed CPM model. Further, increments in individual and collective cell migration upon initiation of intracellular pathways resulting in drastic cytoskeletal deformations (often integrated by activation of proteolytic machinery) is constitutively active in mesenchymal cells, including fibroblasts and solid tumor cells [49, 61, 108, 110, 114], which display prominent protrusions and spindle-shaped morphology. In particular, the ability of tumor cells to undergo continuous morphological changes during motion has a big impact on their invasiveness (and eventually on the overall aggressiveness of the disease), as provided for pancreatic cancer cells (Panc-1) in [106], with a microchannel-based approach, and in [10], with a Boyden chamber assay. In both cases, the authors have in fact correlated an increment in the ability of malignant cells to migrate within selected subcellular structures (microchannel-like chips and microporous membranes, respectively) to a drop in their elastic modulus, measured by micro-plate based single-cell stretchers. All these results are consistent with the outcomes of the proposed CPM simulations although without an explicit definition of the concept of persistent migration.

In the case of a two-component matrix, the proposed CPM simulations have shown that the healing potential of the cell population is significantly enhanced by a proper distribution of collagenous-like fibers. The density of the insoluble part of the matrix as well as the strength of cell-fiber adhesion determine instead a bimodal behavior of culture invasiveness. In this respect, it is useful to underline that model variations either of fiber amount or of $J^{ext}_{C,F}$ are two distinct ways to modulate cell affinity with the fibrous component of the matrix, i.e., through variations either of the number of insoluble ligands or of the expression/activity of integrins, respectively. A biphasic dependence between the migratory capacity of cells and their adhesive affinity with matrix fibrous components has been found in a wide range of experimental works (not necessarily focused on wound healing systems). For instance, a number of 3D assays have shown similar trends for several cell types, including human prostrate carcinoma cells, whose velocity has been plotted as a biphasic function of selected adhesive parameters such as ligands functionality and receptor density [144], and melanoma cells, cultured in collagen scaffolds and stimulated with different concentrations of integrin-binding peptide RGD, which is a tripeptide composed of L-arginine, glycine,

and L-aspartic acid, see [17]. Further, the velocity of primary human fibroblasts coated in synthetic matrix metalloproteinase-sensitive hydrogels has been provided to vary non-linearly with increasing ligand concentrations, as it first increases, reaches a maximum and then decreases [78]. In summary, all these experimental results are in a remarkable accordance with the outcomes of the proposed CPM, as they show that a medium level of both cell-fiber adhesion and of fiber amount is needed for a maximal effectiveness of cell migration. Other studies have demonstrated that individual cell migration on planar substrates (which is fundamental in determining the healing rate of a cell culture) is limited for low fiber densities by the impossibility of cells to form sufficient attachments to generate traction and to move forward [59, 75]. On the other hand, further experimental analysis have shown that, at too dense fibrous matrices, cell movement is inhibited because integrin receptors engage into stable focal adhesions, which hardly break thereby disrupting cell locomotion, as in the case of smooth muscle cells derived from aorta [40] and of fibroblasts [54] coated on collagenous substrates. Coherently, an optimal density of fibers has been provided to result in rapid and coordinated focal adhesion turnovers, which is necessary for a maximal cell movement of cells, see for instance [4, 21, 74, 96] and reference therein.

The effect of cell-substrate adhesion on cell migratory determinants has been analyzed with models of wound healing as well. For instance, matrix substrates modified with increasing concentrations of adhesion ligands such as fibronectin (FN) and Arg-Gly-Asp (RGD) peptides have been shown to facilitate wound closure in the case of endothelial cells [135], fibroblasts [135] and corneal epithelial cells (HCE, [5, 44, 98]). In particular, in [44], HCE sheets have been seeded on bioengineered substrates formed, from the bottom to the top, by a glass coverslip, an artificial extracellular matrix (aECM) containing RGD domains and a fibronectin layer. In this respect, the wound area has been obtained by peeling off a central PDMS barrier: this has permitted to completely remove cells and fibronectin components and to have an exposed aECM in the region deprived of cells. As a result, the authors have observed a minimal invasion at low cell-aECM adhesiveness, given by a low concentration of RGD. On the opposite, a significant increment in wound closure rate has been measured in the case of maximal RGD density. Interestingly, the authors have noticed that increments in the healing capacity result by increments in the number of cells that "decide" to enter the exposed aECM area and not by increments in cell speed. In this respect, Fig. 16 shows a comparison between selected results from CPM

simulations and the outcomes obtained in the paper by Fong and co-workers. In particular, the plot represents the wound edge displacement (at comparable times) in the case of: the simulation setting of Fig. 10, a simulation employing the same matrix substrate as the one used in Fig. 10 but without a chemical stimulation of the virtual culture, and the experiments by Fong and colleagues performed with different densities of RGD domains. A good fitting both in the wound closure rate and in the final edge displacement is achieved between the case of the non-stimulated virtual cell culture and the experiments employing an aECM with a density of RGD grater than 50%. Although there are some relevant differences between *in vitro* and *in silico* settings (for instance, the latter neglect cell proliferation), such a comparison represents a further validation of the model outcomes in the case of a two-component substrate.

The close dependance between cell-fiber adhesiveness and cell migration is not necessarily valid for all cell types. Some cell lineage are in fact able to activate adhesion-independent strategies that allow them to move on or within a collagenous-like networks by unspecific interactions with the lattice or only by cytoskeleton-mediated propulsive mechanisms, see [47] for a review and [50] for a specific study on leukocytes.

The relationship between the efficiency of cell migration and the orientation and spacing of matrix components (and consequently of the adhesive ligands) has been experimentally proven by several experimental models. In [90], a set of wound healing experiments of human umbilical vein endothelial cell (HUVEC) sheets seeded on bioengineered silicon substrates has been analyzed with Cell Image Velocimetry (CIV, a software able to combine an automated detection mechanism for tracing the migrating wound front with a flow detection tool for capturing transport processes inside the cell layer). In a complete agreement with the proposed CPM simulations, an alignment in the topography of the surface in the direction orthogonal to the wound edge has been observed to induce cell shape polarization and orientation and to lead to sustained cell migration, thereby allowing an optimal wound closure. In [90], topographical modifications of the substrates have been obtained with nanoimprint lithography (NIL): lithographic and microprinting techniques have been widely employed also to create one-dimensional ECM pathways able to offer geometric guidance and adhesive structures at a microscale for increasing cell migratory ability [16, 35, 38, 76]. Cell preferential migration along aligned matrix fibers within 3D environments has been analyzed as well for fibroblasts in collagen [33] or neuronal cells in fibrin substrates [37].

Lastly, *in vivo* intravital imaging studies of carcinoma cells in the mammary fat pad have pointed out the preferential chemotactic movement of invasive malignant cells along thick bundles of collagen fibers which behave as guidance cues towards blood vessels [26]. Finally, in the lymph node paracortex, the aligned microarchitecture of collagen and fibronectin fibers ensheathed by fibroblastic reticular cells significantly influences the migratory behavior of T-cells [9].

Comparison with the pertinent computational literature. Wound healing-like scenarios (both *in vitro* and *in vivo*) have been reproduced by several mathematical models as well. In particular, it is possible to distinguish three types of approaches: *fully continuous*, *fully discete* (widely known also as Individual Cell-Based Models (IBMs) or Cellular Automata (CA)), and *hybrid*. The first group includes methods that describe the cell population of interest as a density, with its motility prescribed by a diffusive flux. The resulting behavior of the aggregate satisfies therefore a Fisher equation, characterized by traveling-wave solutions that advance with a speed determined by the diffusion coefficient. In this respect, the diffusivity can be considered either constant or a function of an external chemical factor [28]. Some models of this type also account for cell mitosis and apoptosis: as a consequence, speed and invasive depth of the moving front are further biased by variations in the overall cell mass and therefore depend on the cell duplication/death characteristic times, as in [80, 81, 111, 129]. Finally, continuous approaches can be properly extended by incorporating mechanical aspects of cell traction, as done for instance in [131], where the authors have focused on wound contraction and have compared their predictions with selected results obtained from experiments on rats [87]. This continuous model has been further extended in [93] by including a phenotypic differentiation between fibroblasts and their active contraction-producing form, i.e., the myofibroblasts. With respect to the proposed CPM, the above-described continuous approaches are more suitable to deal with populations composed of a large number of cells, due to their low computational cost. However, they are not able to capture the behavior of individual cells: this impedes, for example, a proper reproduction of cell morphological evolutions as well as of wound invasion by fronts of scattered individuals. Also the phenotypical differentiation between cells located at different distances from the wound edge can not be properly reproduced.

On the opposite, individual-cell based approaches (such as the CPM it-

self) represent each cell of the system of interest as one or a group of spatially-defined units. In [71], a stochastic IBM has described the qualitative behavior of fronts of cells invading a wound. In particular, in that work, cells have been given probabilistic rules for motion and proliferation, which depend on an adhesive parameter. In this respect, the authors have found that different invasive morphologies arise from different ranges both of such a cell-cell adhesive strength and of cell proliferation rate. Interestingly, the same authors have also speculated that their adhesive coefficient can be related to the ratio between the magnetic coupling parameter and the Boltzmann-like temperature characterizing Ising models. These parameters correspond to $J^{exp}_{M,M}$ and $T_{\sigma:\tau(\sigma)=C,M}$ in the present paper (recalling that the CPM is originally based on the Ising approach). In [44], a dynamic Monte Carlo environment has been instead employed to study the role of crossing boundary in an epithelial wound healing, in according to the above-mentioned corresponding experimental observations. In particular, the authors have implemented a master equation with probabilistic rules for cell spreading, retraction and proliferation, where the rate of movement towards the regions with exposed aECM is a function of the RGD density.

Finally, hybrid approaches use an individual-based representation for cells and a continuous approximation for both matrix substrates (with the assumption that collagen-like fibers are at least one order of magnitude smaller that cells) and molecular variables. In this respect, the family of models by Dallon and co-workers has deeply analyzed the relation between the migratory ability of cell aggregates (mainly fibroblasts or dermal cells) and topology and selected structural properties of the extracellular environment. For instance, in [29] cells have been modeled as point particles that move at a constant speed. However, the direction of their movement is governed by the local concentration and disposition of ECM fibers. The assumption made by these authors is consistent with the outcomes of the proposed CPM on the role of fiber alignment in determining the linearity of cell movement (and eventually the overall healing rate of the culture). In this respect, it is useful to remark that in this paper the relation between fiber distribution and cell movement is not prescribed *a priori* but is a self emergent feature of the model. However, Dallon et colleagues have accounted both collagen deposition and fiber reorientation. In [30], the same group of authors have concluded that the most important factor influencing a scar after a lesion is the influx (also in terms of speed) of fibroblasts from the surrounding undamaged tissue. Then, in [31], they have further developed their approach to examine the role of

TGF-β in affecting cell motility, proliferation and collagen production, and therefore ultimately in determining the healing rate. Finally, their more recent paper [86] has included a chemoattractant with a stationary, spatially nonuniform distribution, which is assumed to be produced by leucocytes that have migrated into the wound before fibroblast infiltration. In this respect, the authors have argued that the degree of scarring is maximized at a large chemoattractant diffusion coefficient and minimized in the presence of a chemoattractant inhibitor. The series of models by Dallon and co-workers has developed in [27] by including a cytokine-dependent proliferation, the inhibition of mitosis when space is not available, a tensor-based representation for fibers (which allows to account for the bidirectionality of fiber alignment, neglected in previous similar approaches) and cell-cell interactions, such as collisions and contact inhibition. In particular, these last model features are permitted by representing cells as discrete entities that can occupied not only a node but an extended region of the domain (as happens, for instance, in CPM approaches).

Contact inhibition of movement in wound healing has been the main focus of an interesting model by Cai and co-workers [18]. The authors have first generalized the Fisher equation by defining the diffusivity as a decreasing function of the cell density. The resulting continuous model has been then decomposed to obtained a continuous-in-time discrete-in-space master equation for individual cell behavior. Finally, both copies of the model have been applied to an experimental wound healing system of mice NIH 3T3 fibroblast cells. In this respect, it is interesting to observe that the phenotypic differentiation between external and internal cells (widely described in this CPM) has been captured both by their discrete-in-space approach and by their extended Fisher model.

Possible model developments. The proposed model is highly flexible and could in principle be applied to any cell population stimulated by any motility agent only changing the parameters describing the cell basal properties and regulating the dynamics of the chemical factor involved. For instance, as evident biomedically relevant examples, the application of the proposed approach to an epithelial cell culture would allow to test the physiological conditions in which the recovery of skin lesions is more efficient. On the contrary, its application in the case of malignant cell lines would allow to test potential therapies able to interfere with the ability of tumors to invade and metastasize.

However, the present CPM can of course be improved in several aspects. First, in the present version of the model, certain cell-matrix interactions that greatly affect cell migration both *in vivo* and *in vitro* have not been included, e.g., the ability of individuals to alter their environment by i) the dissolution of insoluble matrix components via the activity of proteases, ii) the deposition of matrix molecules and iii) the remodeling of matrix fibers, mainly caused by tractional forces exerted by the moving cells themselves. In all the presented simulations, the substrate has been in fact assumed static, as cells have been allowed to change the lattice by only occupying sites, which, once abandoned, returned to their initial state. Finally, the importance of either *haptotaxis*, which is the tendency of cells to move along gradients of cell adhesion sites [20], or *durotaxis*, which instead defines the tendency of cells to move towards stiffer regions of a substrate [77], has not been elucidated. The preference for collagen-like components has been in fact described by a single parameter, i.e., $J^{ext}_{M,F}$, which defines the adhesion driven by cell-collagen receptors. This model coefficient can be interpreted as an implicit measure of the haptotactic force. However, it is equally possible to speculate that $J^{ext}_{M,F}$ is determined by the cell preference for moving on a stiff substrate, i.e., by durotaxis. However, the proposed simulations have shown that a cell affinity for the fibrous structure of the matrix (whether haptotactic or durotactic in nature) is sufficient to enhance the invasive capability of the population. A deeper analysis of the mechanical properties of the substrate is however of particular relevance for explaining multiple other aspects of the healing process as well, as provided in [133] in the case of glioma cells.

A further development of the proposed model is its extension to three-dimensional settings, that mimic more appropriately cell migration in *in vivo* conditions. The basic program of collective cell invasion within 3D environments requires not only cell polarization, attachment and propulsion by contraction of cytoskeletal elements, but also cell steering throughout steric obstacles, which typically characterize dense and rigid connective tissues. Cells are able to significantly move within constrained matrix environments by

- drastic morphological deformations, that involve the substantial reorganization both of cell cytoskeleton and of other intracellular organelles, in particular of the nucleus, the most voluminous and rigid intracellular compartment, as described in details in [46, 48, 55, 59, 108, 139, 140];
- activation of localized pericellular proteolysis, able to degrade insolu-

ble matrix components thereby opening space for cell movement (the reader may refer to [62, 102] and again to [108, 139, 140] and references therein).

In this respect, the proposed modeling framework has no intrinsic conceptual limitations for a 3D extension: however, at least a detailed description of the deformation dynamics of cell nucleus (i.e., maybe via a proper visco-elastic mechanical law) as well as a reaction-diffusion equation reproducing the activity of matrix degrading enzymes should be included. In particular, some of these aspects have been analyzed in the already-cited CPMs dealing with single cell migration in confined structures [118, 120]. For the sake of completeness, it has to be underlined that the above-described mechanisms of cell invasion within 3D matrix environments characterize a wide range of collective migratory processes (for example, morphogenesis, angiogenesis or cancer invasion, as reviewed in [45, 47, 66]) and not only wound healing-like phenomena.

Realistic simulations of regenerations of damaged tissues would also require to account for functional differentiations occurring among individuals of the same population. For instance, leader and follower cells emerge during recovery of skin lesions [45]. Obviously, in these cases, it would be necessary to define in the model all cell types, with rules both for their specific behavior and for phenotypic transitions.

Finally, a complete and detailed description of *in vivo* wound healing scenarios should include other component mechanisms, such as selected inflammatory responses [39] and revascularization processes [130].

Acknowledgments

The Author wish to sincerely thank Prof. Ada Funaro and her group of the Laboratory of Immunogenetics at the University of Turin Medical School for providing unpublished experimental results, fundamental for model calibration and validation. The Author also wish to thank Prof. Luigi Preziosi for valuable discussions.

Materials and Methods

Wound healing assay. The experimental setup is analogous to the one described in the work by Ortolan et al. [94]. In particular, NIH:OVCAR-3 cells are grown to

confluence. Then a 700 μm-wide wound is created by scraping the middle of the cell monolayer with a sterile pipette tip. Finally, debris and floating cells are gently rinsed and removed, and RPMI-1640 medium with 1% FCS is added. Wound healing is observed at 0 and 12 hours in the case of NIH:OVCAR-3 cell transfection with a pcDNA3.1 vector containing either full-length CD157 cDNA (*CD157* condition) or not (*MOCK* condition). Images are acquired using an Olympus Biosystems Microscope IX70, equipped with an F-View II camera and AnalySIS FIVE software (Olympus Biosystems).

Data analysis. The position of a virtual cell η is established by calculating the position of its center of mass

$$\mathbf{x}_\eta^{CM}(t) = \frac{\sum_{\mathbf{x}\in\eta} \mathbf{x}}{\sum_{\sigma\in\eta} v_{\eta,\sigma}(t)}.$$

Therefore its path is defined as the path of its center of mass. Coherently, the instantaneous speed of a virtual cell η is established by the instantaneous speed of its center of mass

$$\mathbf{v}_\eta(t) = \frac{\mathbf{x}_\eta^{CM}(t) - \mathbf{x}_\eta^{CM}(t-\Delta t)}{\Delta t},$$

where $\Delta t = 1800$ MCS, as done also in [88, 97]. The mean velocity of η during the entire healing process is instead computed as

$$\mathbf{mv}_\eta = \frac{\mathbf{x}_\eta^{CM}(t_{final}) - \mathbf{x}_\eta^{CM}(0)}{t_{final}},$$

where t_{final} corresponds to the end of the observation period, i.e., after 21600 MCS. Instantaneous and mean velocities are eventually converted in actual unit of measure (μm/s). Both in the experimental and in the simulation setting, the linearity L of migration is obtained by the ratio between the x-component of the final displacement of a cell (x is the axis perpendicular to the wound edge) and its overall displacement at the end of the observation period [82]. The value of L ranges from 0 to 1, being close to 0 when the motion of the cell has no directional trend, and getting larger for motions clustered towards the center of the wound.

Wound healing capacity of the experimental culture is quantified by calculating the mean of 30 randomly chosen intercellular distances across the wound at time 12 hours divided by the initial width of the scratch (700 μm). This value, multiplied by 100 and labeled with D_{exp}, gives a measure of the percentage of the recolonized area of the wound. Coherently, the healing capacity of the virtual population is monitored by measuring

$$D(t) = \frac{d(t)}{d_0} \cdot 100,$$

where d_0 is the initial width of the scratch (175 lattice sites ≈ 350 μm) and $d(t)$ is the average distance between 30 randomly chosen cells at the edge of the wound and the right border of the domain Ω. $D(t_{final})$ indeed quantifies the percentage of wound closure at the end of the simulation: it can therefore be properly compared with the experimental value D_{exp}.

Statistics. For both MOCK and CD157 condition, a single experiment is analyzed for evaluating the final wound closure percentage D_{exp}. On the opposite, the healing capacity of the virtual cell culture, given by D, is obtained by the mean ($\pm$ standard deviation, SD) over 20 independent simulations. The migratory properties of the three cell subpopulations are instead statistically analyzed from a single realization for each simulation setting. In particular, in the circular charts, the final position (given in polar coordinates [7]) of 20 representative cells for each subgroup are represented. The instantaneous velocity, the mean velocity and the linearity (also for the experimental assay) are instead averaged (with SD) over 30 randomly chosen cells.

Model parameter estimates. The proposed model deals with a generic cell population stimulated by a generic chemical factor. Therefore, the set of parameter estimates is assembled from a composite set of data. However, the behavior of the computational results is fairly robust in a large region of the parameter space around such estimates. A summary of parameter values used in the model is given in Table 1, while in this section some details of how they are estimated is provided. The initial/target dimensions of cells represent the standard mean measures of an eukariotic cell [2]. The cell basal properties have not a direct correspondence with specific experimental quantities. However, it is possible to heuristically infer their estimates with realistic biological observations. T_0 represents the cell intrinsic motility in resting conditions: assuming that the simulated cell line is characterized by a low basal migratory capacity, a low $T_0 = 4.5$ can be set. T_N models instead the passive movement of cell nucleus: therefore it is obvious that $T_N < T_0$. In particular, after some trials, a reasonable value $T_N = 1$ can be found (lower values result in the complete inhibition of cell movement, as the nucleus is almost "frozen"). Since the model does not account for any nutrients, in order to keep fluctuations of cell volume within a few percent, a high $\kappa = 20$ is set. ν measures both the compressibility of cell nucleus and the intrinsic cell elasticity. Assuming that without chemical stimulations cells do not significantly remodel a high $\nu = 20$ is also set. $J^{int}_{C,N}$ and $J^{int}_{C,M}$ are the generalized contact tensions between intracellular compartments. High negative $J^{int}_{C,N} = J^{int}_{C,M} = -20$ are chosen to prevent cells from disconnecting, see [116]. The J^{ext}s represent instead the real adhesive strengths of the cells. As it is widely demonstrated in literature (see for instance [125] and references therein), cells of a wide range of lines in standard

conditions preferentially adhere to each other (via cadherin-cadherin junction) or with the fibrous component of the extracellular environment (via integrin ligand), while they experience substantially low adhesive interactions with the undifferentiated, gelatinous component of coating matrices. Therefore, after trying a wide range of values, a reasonable option is the hierarchy $J^{ext}_{M,M} = J^{ext}_{M,F} = 4.5$ and $J^{ext}_{M,Q} = 7$. This choice also assures that, in the case of resting conditions, the population does not unrealistically expand as a consequence of an unjustified intercellular repulsion. Moreover, $J^{ext}_{M,M}$ and $J^{ext}_{M,F} = 4.5$ are set equal to the intrinsic cell motility T_0 to ensure a good balance between the most relevant forces acting on the non-stimulated cell culture. Finally, the basal intracellular concentration of the chemical c_0 is assumed homogeneous within each cell and equal to 0.05 μM.

The conversion between simulation time and experimental time is found by an empirical calibration between computational outcomes and corresponding experimental results, as done in [44]. In more details, the wound closure percentages obtained from CPM simulations for different final observation times (i.e., for different numbers of run MCS) are fitted with the values of D_{exp} evaluated from the experiments by Ortolan et al. in the corresponding conditions (i.e., non-stimulated virtual cell culture vs. MOCK experimental cell culture and chemically stimulated virtual cell culture vs. CD157-transfected experimental cell culture). By using this approach, 21600 MCS are observed to correspond to 12 hours, as indicated by the gray shadow in the plot of Fig. 17, and therefore 1 MCS corresponds to nearly 2 seconds.

Such a temporal conversion, along with the characteristic size of each lattice site (i.e., 2 μm), leads to the following set of values for the chemical kinetics: $s_c = 0.5$ h^{-1}, $D = 10$ $\mu\mathrm{m}^2\mathrm{s}^{-1}$, and $\lambda = 2 \cdot 10^{-4}$ s^{-1}. In this respect, the obtained estimates are consistent with the values measured for the most studied growth factors (i.e., vascular endothelial growth factor isoforms [121] and hepatocyte growth factor [32]).

Table 1: Summary of the parameters used in the CPM simulations.

Parameter	Description	Value [Units]	Reference(s)
V_N	volume of nuclear compartment	50 [μm^2]	[2]
S_N	surface of nuclear compartment	43 [μm]	[2]
V_C	volume of cytosolic compartment	150 [μm^2]	[2]
S_C	surface of cytosolic compartment	90 [μm]	[2]
V_M	volume of plasma membrane	60 [μm^2]	[2]
S_M	surface of plasma membrane	60 [μm]	[2]
T_0	basal cell motility	4.5	estimated
T_N	generalized motility of the nucleus	1	estimated
h	Michaelis-Menten coefficient for T	1/3	estimated
κ	basal volume elasticity	20	estimated
ν	basal surface elasticity	20	estimated
$J^{int}_{(C,N),(C,M)}$	intracellular contact tensions	-20	[116]
$J^{ext}_{M,M}$	basal cell-cell adhesive strength	4.5	estimated
$J^{ext}_{M,F}$	basal cell-fibers adhesive strength	4.5	estimated
$J^{ext}_{M,Q}$	basal cell-medium adhesive strength	7	estimated
j	coefficient for $J^{ext}_{M,M}$	1/2	estimated
D	diffusion constant of chemical	10 [μm^{2}s^{-1}]	[32, 121]
λ	on-rate constant of chemical degradation	$2 \cdot 10^{-4}$ [s^{-1}]	[32, 121]
s_c	on-rate constant of chemical addition	0.5 [h^{-1}]	estimated
β	maximum rate of chemical uptake	0.06 [pg/(cell h)]	[8, 79]
k	coefficient of chemical uptake rate	1 [h^{-1}]	estimated
c_0	basal intracellular level of chemical	0.05 [μM]	estimated

[1] Abercrombie M. The crawling movement of cells. Proc R Soc London B, 1980; 207: 129 - 47.

[2] Alberts B, Bray D, Lewis J, Raff M, Roberts K, Watson JD. Molecular Biology of the Cell, 3rd ed. Garland Science; 1994.

[3] Aman A, Piotrowski T. Wnt/beta-catenin and Fgf signaling control collective cell migration by restricting chemokine receptor expression. Dev Cell, 2008; 15: 749 – 61.

[4] Arnold M, Hirschfeld-Warneken VC, Lohmüller T, Heil P, Blümmel J, Cavalcanti-Adam EA, López-Garca M, Walther P, Kessler H, Geiger B, Spatz JP. Induction of cell polarization and migration by a gradient of nanoscale variations in adhesive ligand spacing. Nano Lett, 2008; 8: 2063 - 9.

[5] Aucoin L, Griffith CM, Pleizier G, Deslandes Y, Sheardown H. Interactions of corneal epithelial cells and surfaces modified with cell adhesion peptide combinations. J Biomat Sci-Polym E, 2002; 13: 447 - 62.

[6] Balter A, Merks RMH, Poplawski NJ, Swat M, Glazier JA. The Glazier-Graner-Hogeweg model: extensions, future directions, and opportunities for further study. In Anderson ARA, Chaplain MAJ, Rejniak KA, Eds. Single-Cell-Based Models in Biology and Medicine, Mathematics and Biosciences in Interactions. Birkaüser 2007; pp 151 – 67.

[7] Batschelet E. Circular statistics in biology. London, UK, Academic Press; 1981.

[8] Bauer AL, Jackson TL, Jiang Y. A cell-based model exhibiting branching and anastomosis during tumor-induced angiogenesis. Biophys J, 2007; 92: 3105 – 21.

[9] Bajnoff M, Egen JG, Koo LY, Laugier JP, Brau F, Glaichenhaus N, Germain RN. Stromal cell networks regulate lymphocyte entry, migration, and territoriality in lymph nodes, Immunity, 2006; 25: 989 - 1001.

[10] Beil M, Micoulet A, von Wichert G, Paschke S, Walther P, Omary MB, Van Veldhoven PP, Gern U, Wolff-Hieber E, Eggermann J, Waltenberger J, Adler G, Spatz J, Seufferlein T. Sphingosylphosphorylcholine regulates keratin network architecture and viscoelastic properties of human cancer cells. Nat Cell Biol, 2003; 5: 803 – 11.

[11] Bement W, Forscher P, Mooseker M. A novel cytoskeletal structure involved in purse string wound closure and cell polarity maintenance. J Cell Biol, 1993; 121: 565 – 78.

[12] Bennett J, Weeds A. Calcium and the cytoskeleton. Br Med Bull, 1986; 42: 385 – 90.

[13] Block ER, Matela AR, SundarRaj N, Iszkula ER, Klarlund JK. Wounding induces motility in sheets of corneal epithelial cells through loss of spatial constraints. Roles of heparin-binding epidermal growth factor-like signaling. J Biol Chem, 2004; 279: 24307 - 12.

[14] Brightman AO, Rajwa BP, Sturgis JE, McCallister ME, Robinson JP, Voytik-Harbin SL. Time-lapse confocal reflection microscopy of collagen fibrillogenesis and extracellular matrix assembly in vitro. Biopolymers, 2000; 54: 222 – 34.

[15] Brock J, Midwinter K, Lewis J, Martin P. Healing of incisional wounds in the embryonic chick wing bud: characterization of the actin purse-string and demonstration of a requirement for Rho activation. J Cell Biol, 1996; 135: 1097 – 107.

[16] Brock A, Chang E, Ho CC, LeDuc P, Jiang X, Whitesides GM, Ingber DE. Geometric determinants of directional cell motility revealed using microcontact printing, Langmuir, 2003; 19: 1611 – 7.

[17] Burgess BT, Myles JL, Dickinson RB. Quantitative analysis of adhesion-mediated cell migration in three-dimensional gels of RGD-grafted collagen. Ann Biomed Eng, 2003; 28: 110 – 8.

[18] Cai AQ, Landman KA, Hughes BD. Multi-scale modeling of a wound-healing cell migration assay. J Theor Biol, 2007; 245: 576 – 94.

[19] Capito RM, Spector M. Scaffold-based articular cartilage repair. IEEE Eng Med Biol Mag, 2003; 22: 42 – 50.

[20] Carter SB. Haptotaxis and the mechanism of cell motility, Nature, 1967; 213: 256 – 60.

[21] Cavalcanti-Adam EA, Volberg T, Micoulet A, Kessler H, Geiger B, Spatz JP. Cell spreading and focal adhesion dynamics are regulated by spacing of integrin ligands. Biophys J, 2007; 92: 2964 - 74.

[22] Cavallaro U, Christofori G. Cell adhesion in tumor invasion and metastasis: loss of the glue is not enough. Biochim Biophys Acta, 2001; 1552: 39 - 45

[23] Cavallaro U, Christofori G. Cell adhesion and signalling by cadherins and Ig-CAMs in cancer. Nat Rev Cancer, 2004; 4: 118 - 32.

[24] Chen N, Glazier JA, Izaguirre JA, Albera MS. A parallel implementation of the Cellular Potts Model for simulation of cell-based morphogenesis. Comput Phys Commun, 2007; 176: 670 – 81.

[25] Christofori G. Changing neighbours, changing behaviour: cell adhesion molecule-mediated signalling during tumour progression. EMBO J, 2003; 22: 2318 - 23.

[26] Condeelis J, Segall JE. Intravital imaging of cell movement in tumours, Nat Rev Cancer, 2003; 3: 921 – 930.

[27] Cumming BD, McElwain DLS, Upton Z. A mathematical model of wound healing and subsequent scarring. J R Soc Interface, 2010; 7: 19 - 34.

[28] Dale PD, Maini PK, Sherratt JA. Mathematical modeling of corneal epithelial wound healing. Math Biosci, 1994; 124: 127 – 47.

[29] Dallon JC, Sherratt JA, Maini PK. Mathematical modelling of extracellular matrix dynamics using discrete cells: fiber orientation and tissue regeneration. J Theor Biol, 1999; 199: 449 – 71.

[30] Dallon JC, Sherratt JA, Maini PK, Ferguson M. Biological implications of discrete mathematical model for collagen deposition and alignment in dermal wound repair. J Math Appl Med Biol, 2000; 17: 379 – 93.

[31] Dallon JC, Sherratt JA, Maini PK. Modeling the effects of transforming growth factor-b on extracellular matrix alignment in dermal wound repair. Wound Repair Regen, 2001; 9: 278 – 86.

[32] De Luca A, Arena N, Sena LM, Medico E. Met overexpression confers HGF-dependent invasive phenotype to human thyroid carcinoma cells in vitro. J Cell Physiol, 1999; 180: 365 – 71.

[33] Dickinson RB, Guido S, Tranquillo RT. Biased cellmigration of fibroblasts exhibiting contact guidance in oriented collagen gels. Ann Biomed Eng, 1994; 22: 342 – 56.

[34] Di Renzo MF, Oliviero M, Narsimhan RP, Bretti S, Giordano S, Medico E, Gaglia P, Zara P, Comoglio PM. Expression of the Met/HGF receptor in normal and neoplastic human tissues. Oncogene, 1991; 6: 1997 – 2003.

[35] Doyle AD, Wang FW, Matsumoto K, Yamada KM. One-dimensional topography underlies three-dimensional fibrillar cell migration. J Cell Biol, 2009; 84: 481 – 90.

[36] Drake CJ, LaRue A, Ferrara N, Little CD. VEGF regulates cell behavior during vasculogenesis. Dev Biol, 2000; 224: 178 – 88.

[37] Dubey N, Letourneau, PC, Tranquillo RT. Neuronal contact guidance in magnetically aligned fibrin gels: effect of variation in gel mechano-structural properties. Biomaterials, 2001; 22: 1065 – 75.

[38] Dunn GA, Ebendal T. Contact guidance on oriented collagen gels. Exp Cell Res, 1978; 111: 475 – 9.

[39] Eming SA, Krieg T, Davidson JM. Inflammation in wound repair: molecular and cellular mechanisms. J Invest Dermatol, 2007; 127: 514 – 25.

[40] Engler A, Bacakova L, Newman C, Hategan A, Griffin M, Discher D. Substrate compliance versus ligand density in cell on gel responses. Biophys J, 2004; 86: 617 – 28.

[41] Farooqui R, Fenteany G. Multiple rows of cells behind an epithelial wound edge extend cryptic lamellipodia to collectively drive cellsheet movement. J Cell Sci, 2005; 118: 51 – 63.

[42] Fenteany G, Janmey PA, Stossel TP. Signaling pathways and cell mechanics involved in wound closure by epithelial cell sheets. Curr Biol, 2000; 10: 831 – 8.

[43] Ferrero E, Saccucci F, Malavasi F. The human CD38 gene: polymorphism, CpG island, and linkage to the CD157 (BST-1) gene. Immunogenetics, 1999; 49: 597 - 604.

[44] Fong E, Tzlilb S, Tirrell DA. Boundary crossing in epithelial wound healing. Proc Natl Acad Sci USA, 2010; 107: 19302 - 7.

[45] Friedl P, Gilmour D. Collective cell migration in morphogenesis, regeneration and cancer. Nat Rev Mol Cell Biol, 2009; 10: 445 – 57.

[46] Friedl P, Brocker EB. The biology of cell locomotion within three dimensional extracellular matrix. Cell Mol Life Sci, 2000; 57: 41 – 64.

[47] Friedl P, Wolf K. Tumour-cell invasion and migration: diversity and escape mechanisms. Nat Rev Cancer, 2003; 3: 362 – 74.

[48] Friedl P, Wolf K, Lammerding J. Nuclear mechanics during cell migration. Curr Opin Cell Biol, 2011; 23: 253.

[49] Friedl P, Alexander S. Cancer invasion and the microenvironment: plasticity and reciprocity. Cell, 2011; 147: 992 - 1009

[50] Friedl P, Entschladen F, Conrad C, Niggemann B, Zänker KS. CD4+ T-lymphocytes migrating in three-dimensional collagen lattices lack focal adhesions and utilize $\beta 1$ integrin-independent strategies for polarization, interaction with collagen fibers and locomotion. Eur J Immunol, 1998; 28: 2331 - 43.

[51] Funaro A, Ortolan E, Ferranti B, Gargiulo L, Notaro R, Luzzatto L, Malavasi F. CD157 is an important mediator of neutrophil adhesion and migration. Blood, 2004; 104: 4269 - 78.

[52] Funaro A, Ortolan E, Bovino P, Lo Buono N, Nacci G, Parrotta R, Ferrero E, Malavasi F. Ectoenzymes and innate immunity: the role of human CD157 in leukocyte trafficking. Front Biosci, 2009; 14: 929 - 43.

[53] Gaggioli C, Hooper S, Hidalgo-Carcedo C, Grosse R, Marshall JF, Harrington K, Sahai E. Fibroblast-led collective invasion of carcinoma cells with differing roles for RhoGTPases in leading and following cells. Nat Cell Biol, 2007; 9: 1392 – 1400.

[54] Gaudet C, Marganski WA, Kim S, Brown CT, Gunderia V, Dembo M, Wong JY. Influence of type I collagen surface density on fibroblast spreading, motility, and contractility. Biophys J, 2003; 85: 3329 - 35.

[55] Gerlitz G, Bustin M. The role of chromatin structure in cell migration. Trends Cell Biol, 2011; 21: 6 - 11.

[56] Giverso C, Scianna M, Preziosi L, Lo Buono N., Funaro A. Individual cell-based model for in-vitro mesothelial invasion of ovarian cancer. Math Model Nat Phenom, 2010; 5: 203 – 23.

[57] Glazier JA, Balter A, Poplawski NJ. Magnetization to morphogenesis: A brief history of the Glazier-Graner-Hogeweg model. In Anderson ARA, Chaplain MAJ, Rejniak KA, Eds. Single-Cell-Based Models in Biology and Medicine, Mathematics and Biosciences in Interactions. Birkaüser 2007; pp 79 – 106.

[58] Glazier JA, Graner F. Simulation of the differential adhesion driven rearrangement of biological cells. Physical Rev E, 1993, 47: 2128 – 54.

[59] Goodman SL, Risse G, Vondermark K. The E8 subfragment of laminin promotes locomotion of myoblasts over extracellularmatrix. J Cell Biol, 1989; 109: 799 – 809.

[60] Graner F, Glazier JA. Simulation of biological cell sorting using a two dimensional extended Potts model. Phys Rev Lett, 1992; 69: 2013 – 17.

[61] Grinnell F, Petroll WM. Cell motility and mechanics in three-dimensional collagen matrices. Ann Rev Cell Dev Bio, 2010; 26: 335 - 61.

[62] Harley BA, Spilker MH, Wu JW, Asano K, Hsu HP, Spector M, Yannas IV. Optimal degradation rate for collagen chambers used for regeneration of peripheral nerves over long gaps. Cells Tissues Organs, 2008; 176: 153 – 65.

[63] Hegedus B, Marga F, Jakab, K, Sharpe-Timms KL, Forgacs G. The interplay of cell-cell and cell-matrix interactions in the invasive properties of brain tumors. Biophys J, 2006; 91: 2708 – 16.

[64] Hegerfeldt Y, Tusch M, Brocker EB, Friedl P. Collective Cell Movement in Primary Melanoma Explants: Plasticity of Cell-Cell Interaction, β1-Integrin Function, and Migration Strategies. Cancer Research, 2002; 65: 2125 – 30.

[65] Horwitz AR, Parsons JT. Cell biology: Cell migration-moving on. Science, 1999; 286: 1102 – 3.

[66] Ilina O, Friedl P. Mechanisms of collective cell migration at a glance J Cell Sci, 2009; 122: 3203 – 8.

[67] Ilina O, Bakker GJ, Vasaturo A, Hofmann RM, Friedl P. Two-photon laser-generated microtracks in 3D collagen lattices: principles of MMP-dependent and - independent collective cancer cell invasion. Phys Biol, 2011; 8: 015010 (2011).

[68] Ishihara K, Hirano T. BST-1/CD157 regulates the humoral immune responses in vivo. Chem Immunol, 2000; 75: 235 - 55.

[69] Ising E. Beitrag zur theorie des ferromagnetismus. Z Physik, 1925; 31: 253.

[70] Itoh M, Ishihara K, Hiroi T, Lee BO, Maeda H, Iijima H, Yanagita M, Kiyono H, Hirano T. Deletion of bone marrow stromal cell antigen-1 (CD157) gene impaired systemic thymus independent-2 antigen-induced IgG3 and mucosal TD antigen-elicited IgA responses. J Immunol, 1998; 161: 3974 - 83.

[71] Khain E, Sander LM, Schneider-Mizell CM. The role of cell-cell adhesion in wound healing. J Stat Phys, 2007; 128: 209 18.

[72] Kimura K, Nishimura T, Satoh Y. Effects of ATP and its analogues on Ca2+ dynamics in the rabbit corneal epithelium. Arch Histol Cytol, 1999; 62: 129 - 38.

[73] Klepeis VE, Weinger I, Kaczmarek E, and Trinkaus-Randal V. P2Y receptors play a critical role in epithelial cell communication and migration. J Cell Biochem, 2004; 93: 1115 - 33.

[74] Lamers E, van Horssen R, te Riet J, van Delft FC, Luttge R, Walboomers XF, Jansen JA. The influence of nanoscale topographical cues on initial osteoblast morphology and migration. Eur Cell Mater, 2010; 9: 329 - 43.

[75] Lauffenburger DA, Lindermann JJ. Receptors: bodels for binding, trafficking, and Signaling. Oxford University Press (1996).

[76] Lehnert D, Wehrle-Haller B, David C, Weiland U, Ballestrem C, Imhof BA, Bastmeyer M, Cell behaviour on micropatterned substrata: limits of extracellular matrix geometry for spreading and adhesion. J Cell Sci, 2004; 117: 41 – 52.

[77] Lo CM, Wang HB, Dembo M, Wang YL. Cell movement is guided by the rigidity of the substrate. Biophys J, 2000; 79: 144 – 52.

[78] Lutolf MP, Lauer-Fields JL, Schmoekel HG, Metters AT, Weber FE, Fields GB, Hubbell JA. Synthetic matrix metalloproteinase-sensitive hydrogels for the conduction of tissue regeneration: engineering cell-invasion characteristics. Proc Natl Acad Sci USA, 2003; 100: 5413 – 8.

[79] Mahoney AW, Smith BG, Flann NS, Podgorski GJ. Discovering novel cancer therapies: a computational modeling and search approach. IEEE Symposium on Computational Intelligence in Bioinformatics and Computational Biology, 233 – 40, 2008.

[80] Maini PK, McElwain DLS, Leavesley D. Travelling waves in a wound healing assay. Appl Math Lett, 2004; 17: 575 – 80.

[81] Maini PK, McElwain DLS, Leavesley D. Travelling wave model to interpret a wound-healing cell migration assay for human peritoneal mesothelial cells. Tissue Eng, 2004; 10: 475 – 82.

[82] Mardia KV, Jupp PE. Directional Statistics. John Wiley and Sons, Chichester, UK; 2000.

[83] Marée AFM, Grieneisen VA, Hogeweg P. The Cellular Potts Model and biophysical properties of cells, tissues and morphogenesis. In Anderson ARA, Chaplain MAJ, Rejniak KA, Eds. Single-Cell-Based Models in Biology and Medicine, Mathematics and Biosciences in Interactions. Birkaüser 2007; pp 107 – 36.

[84] Martin P, Lewis J. Actin cables and epidermal movement in embryonic wound healing. Nature, 1992; 360: 179 – 83.

[85] Martin P. Wound healing – aiming for perfect skin regeneration. Science. 1997; 276: 75 – 81.

[86] McDougall S, Dallon JC, Sherratt JA, Maini PK. Fibroblast migration and collagen deposition during dermal wound healing: mathematical modelling and clinical implications. Phil Trans R Soc A, 2006; 364: 1385 – 405.

[87] McGrath MH, Simon RH. Wound geometry and the kinetics of contraction. Plast. Resconstr Surg, 1983; 72, 66 - 72.

[88] Merks RMH, Perryn ED, Shirinifard A, Glazier JA. Contact-inhibited chemotactic motility: role in de novo and sprouting blood vessel growth. PLOS Comp Biol, 2008; 4: e1000163.

[89] Metropolis N, Rosenbluth AE, Rosenbluth MN, Teller AH, Teller E. Equation of state calculations by fast computing machines. J Chem Phys, 1953; 21: 1087 – 92.

[90] Milde F, Franco D, Ferrari A, Kurtcuoglu V, Poulikakos D, Koumoutsakos P. Cell Image Velocimetry (CIV): boosting the automated quantification of cell migration in wound healing assays. Integr Biol (Camb), 2012; 4: 1437 – 47.

[91] Mogilner A, Oster G. Polymer motors: Pushing out the front and pulling up the back. Current Biology, 2003; 13: R721 – 33.

[92] Nikolić DL, Boettiger AN, Bar-Sagi D, Carbeck JD, Shvartsman SY. Role of boundary conditions in an experimental model of epithelial wound healing. Am J Physiol Cell Physiol, 2006; 291: C68 – 75.

[93] Olsen L, Maini PK, Dallon JC, Sherratt, JA. Mathematical modelling of anisotropy in fibrous connective tissue. Math Biosci, 1998; 158: 145 - 70.

[94] Ortolan E, Arisio R, Morone S, Bovino P, Lo-Buono N, Nacci G, Parrotta R, Katsaros D, Rapa I, Migliaretti G, Ferrero E, Volante M, Funaro A. Functional role and prognostic significance of CD157 in ovarian carcinoma.J Natl Cancer Inst, 2010; 102: 1160 – 77.

[95] Ortolan E, Vacca P, Capobianco A, Armando E, Crivellin F, Horenstein A, Malavasi F. CD157, the Janus of CD38 but with a unique personality. Cell Biochem Funct, 2002; 20: 309 - 22.

[96] Palecek SP, Loftus JC, Ginsberg MH, Lauffenburger DA, Horwitz AF. Integrin-ligand binding properties govern cell migration speed through cell-substratum adhesiveness. Nature, 1997; 385: 537 – 40.

[97] Perryn ED, Czirok A, Little CD. Vascular sprout formation entails tissue deformations and VE-cadherin dependent cell-autonomous motility. Dev Biol, 2008; 313: 545 – 55.

[98] Pettit DK, Hoffman AS, Horbett TA. Correlation between corneal epithelial cell outgrowth and monoclonal antibody binding to the cell binding domain of adsorbed fibronectin. J Biomed Mater Res, 1994; 28: 685 - 91.

[99] Pollard TD, Borisy GG. Cellular motility driven by assembly and disassembly of actin filaments. Cell, 2003; 112: 453 – 65.

[100] Potts RB. Some generalized order-disorder transformations. Proc Camb Phil Soc, 1952; 48: 106 – 9.

[101] Poujade M. Grasland-Mongrain E, Hertzog A, Jouanneau J, Chavrier P, Ladoux B, Buguin A, Silberzan P. Collective migration of an epithelial monolayer in response to a model wound. Proc Natl Acad Sci USA, 2007; 104: 15988 - 93.

[102] Raeber GP, Lutolf MP, Hubbell JA. Molecularly engineered PEG hydrogels: a novel model system for proteolytically mediated cell migration. Biophys J, 2005; 89: 1374 – 88.

[103] Raub CB, Suresh V, Krasieva T, Lyubovitsky J, Mih JD, Putnam AJ, Tromberg BJ, George SC. Noninvasive assessment of collagen gel microstructure and mechanics using multiphoton microscopy. Biophys J, 2007; 92: 2212 – 22.

[104] Ridley AJ, Schwartz MA, Burridge K, Firtel RA, Ginsberg MH, Borisy G, Parsons JT, Horwitz AR. Cell migration: integrating signals from front to back. Science, 2003; 302: 1704 – 9.

[105] Roeder BA, Kokini K, Sturgis JE, Robinson JP, Voytik-Harbin SL. Tensile mechanical properties of three-dimensional type I collagen extracellular matrices with varied microstructure. J Biomech Eng, 2002; 124: 214 – 22.

[106] Rolli CG, Seufferlein T, Kemkemer R, Spatz JP. Impact of Tumor Cell Cytoskeleton Organization on Invasiveness and Migration: A Microchannel-Based Approach. PLoS ONE, 2010; 5: e8726.

[107] Rubenstein BM, Kaufman LJ. The Role of Extracellular Matrix in Glioma Invasion: A Cellular Potts Model Approach. Biophys J, 2008; 95: 5661 – 80.

[108] Sabeh F, Shimizu-Hirota R, Weiss SJ. Protease-dependent vs. -independent cancer cell invasion programs: three dimensional amoeboid movement revisited. J Cell Biol, 2009; 185: 11 - 19.

[109] Sammak PJ, Hinman LE, Tran POT, Sjaastad MD, Machen TE. How do injured cells communicate with the surviving cell monolayer? J Cell Sci, 1997; 110: 465 - 75.

[110] Sanz-Moreno V, Gadea G, Ahn J, Paterson H, Marra P, Pinner S, Sahai E, Marshall CJ. Rac activation and inactivation control plasticity of tumor cell movement. Cell, 2008; 135: 510 - 23.

[111] Savla U, Olson LE, Waters CM. Mathematical modeling of airway epithelial wound closure. J Appl Physiol, 2004; 96: 566 – 74.

[112] Schmidt S, Friedl P. Interstitial cell migration: integrin-dependent and alternative adhesion mechanisms. Cell Tissue Res, 2010; 339: 83 - 92.

[113] Schmidt M, Paes K, De Maziere A, Smyczek T, Yang S, Gray A, French D, Kasman I, Klumperman J, Rice DS. EGFL7 regulates the collective migration of endothelial cells by restricting their spatial distribution. Development, 2007; 134: 2913 – 23.

[114] Schoumacher M, Goldman RD, Louvard D, Vignjevic DM. Actin, microtubules, and vimentin intermediate filaments cooperate for elongation of invadopodia. J Cell Bio, 2010; 189: 541 - 56.

[115] Scianna M, Munaron L, Preziosi L. A multiscale hybrid approach for vasculogenesis and related potential blocking therapies. Prog Biophys Mol Biol, 2011; 106: 450 – 62.

[116] Scianna M, Preziosi L. Multiscale Developments of the Cellular Potts Model. Multiscale Model Simul, 2012; 10: 342 – 82.

[117] Scianna M, Preziosi L. Cellular Potts models: multiscale developments and biological applications. Chapman and Hall/CRC Press (2013).

[118] Scianna M, Preziosi L, Wolf K. A cellular Potts model simulating cell migration on and in matrix environments. Math Biosci Eng, 2013; 10: 235 – 261.

[119] Scianna M, Preziosi L. Modelling the influence of nucleus elasticity on cell invasion in fiber networks and microchannels. J Theor Biol, 2013; 317: 394 – 406.

[120] Scianna M, Preziosi L. A cellular Potts model for the mmp-dependent and -independent cancer cell migration in matrix microtracks of different dimensions. Computational Mechanics, 2014 53: 485 – 497.

[121] Serini G, Ambrosi D, Giraudo E, Gamba A, Preziosi L, Bussolino F. Modeling the early stages of vascular network assembly. EMBO J, 2003; 22: 1771 – 9.

[122] Spadaccio C, Rainer A, De Porcellinis S, Centola M, De Marco F, Chello M, Trombetta M, Genovese JA. A G-CSF functionalized PLLA scaffold for wound repair: An in vitro preliminary study. Conf Proc IEEE Eng Med Biol Soc, 2010: 843 – 6.

[123] Steinberg MS. Reconstruction of tissues by dissociated cells. Some morphogenetic tissue movements and the sorting out of embryonic cells may have a common explanation. Science, 1963; 141: 401 – 8.

[124] Steinberg MS. Does differential adhesion govern self-assembly processes in histogenesis? Equilibrium configurations and the emergence of a hierarchy among populations of embryonic cells. J Exp Zool, 1970; 173: 395 – 433.

[125] Stupack DG. The biology of integrins. Oncology, 2007; 21: 6 – 12.

[126] Sun Y, Chen CS, Fu J. Forcing stem cells to behave: A biophysical perspective of the cellular microenvironment. Ann Rev Biophys, 2012; 41: 519 - 42.

[127] Sundfeldt K. Cell–cell adhesion in the normal ovary and ovarian tumors of epithelial origin; an exception to the rule. Molecular and Cellular Endocrinology, 2003; 202: 89 - 96.

[128] Suzuki K, Saito J, Yanai R, Yamada N, Chikama T, Seki K, Nishida T. Cell–matrix and cell–cell interactions during corneal epithelial wound healing. Prog Retin Eye Res, 2003; 22: 113– 33.

[129] Takamizawa K, Niu S, Matsuda T. Mathematical simulation of unidirectional tissue formation: in vitro transanastomotic endothelialization model. J Biomater Sci Polym Ed, 1997; 8: 323 – 34.

[130] Tonnesen MG, Feng X, Clark RA. Angiogenesis in wound healing. J Investig Dermatol Symp Proc, 2000; 5: 40 – 6.

[131] Tranquillo RT, Murray JM. Continuum model of fibroblast-driven wound contraction: inflammation–mediation. J Theor Biol, 1992; 158: 135 – 72.

[132] Tremel A. Cell migration and proliferation during monolayer formation. Experimental Semester Thesis, Department of Chemical and Biomolecular Engineering, The University of Melbourne, 2006.

[133] Ulrich TA, De Juan Pardo EM, Kumar S. The mechanical rigidity of the extracellular matrix regulates the structure, motility, and proliferation of glioma cells. Cancer Res, 2009; 69: 4167 – 74.

[134] Van Nieuw Amerongen GP, Koolwijk P, Versteilen A, Van Hinsbergh VWM. Involvement of RhoA/Rho kinase signaling in VEGF-induced endothelial cell migration and angiogenesis in vitro. Arteriosclerosis, Thrombosis, and Vascular Biology, 2003; 23: 211 – 7.

[135] Van Horssen R, Galjart N, Rens JAP, Eggermont AMM, ten Hagen TLM. Differential effects of matrix and growth factors on endothelial and fibroblast motility: Application of a modified cell migration assay. J Cell Biochem, 2006; 99: 1536 – 52.

[136] Vleminckx K, Vakaet L, Mareel M, Fiers W, Vanroy F. Genetic manipulation of E-cadherin expression by epithelial tumor cells reveals an invasion suppressor role. Cell, 1991; 66: 107 - 19.

[137] Weidner KM, Behrens J, Vandekerckhove J, Birchmeier W. Scatter factor: molecular characteristics and effect on the invasiveness of epithelial cells. J Cell Biol, 1990; 111: 2097 – 108.

[138] Wolf K, Wu YI, Liu Y, Geiger J. Tam E. Multi-step pericellular proteolysis controls the transition from individual to collective cancer cell invasion. Nat Cell Biol, 2007; 9: 893 – 904.

[139] Wolf K, Friedl P. Extracellular matrix determinants of proteolytic and non-proteolytic cell migration. Trends Cell Biol, 2011; 21: 736 - 44.

[140] Wolf K, Mazo I, Leung H, Engelke K, Von Andrian UH, Deryugina EI, Strongin AY, Brocker EB, Friedl P. Compensation mechanism in tumor cell migration mesenchymal–amoeboid transition after blocking of pericellular proteolysis. J Cell Biol, 2003; 160: 267 - 77.

[141] Xu KP, Ding Y, Ling J, Dong Z, Yu FS. Wound-induced HB-EGF ectodomain shedding and EGFR activation in corneal epithelial cells. Invest Ophthalmol Vis Sci, 2004; 45: 813 - 20.

[142] Yannas IV, Lee E, Orgill DP, Skrabut EM, Murphy GF. Synthesis and characterization of a model extracellular matrix that induces partial regeneration of adult mammalian skin. Proc Natl Acad Sci USA, 1989; 86: 933 – 7.

[143] Zahm JM, Kaplan H, Herard A, Doriot F, Pierrot D, Somelette P, Puchelle E. Cell migration and proliferation during the in vitro repair of the respiratory epithelium. Cell Motil Cytoskel, 1997; 37: 33 – 43.

[144] Zaman MH, Trapani LM, Sieminski AL, Mackellar D, Gong H, Kamm RD, Wells A, Lauffenburger DA, Matsudaira P. Migration of tumor cells in 3D matrices is governed by matrix stiffness along with cell-matrix adhesion and proteolysis. Proc Natl Acad Sci USA, 2006; 103: 10889 - 94.

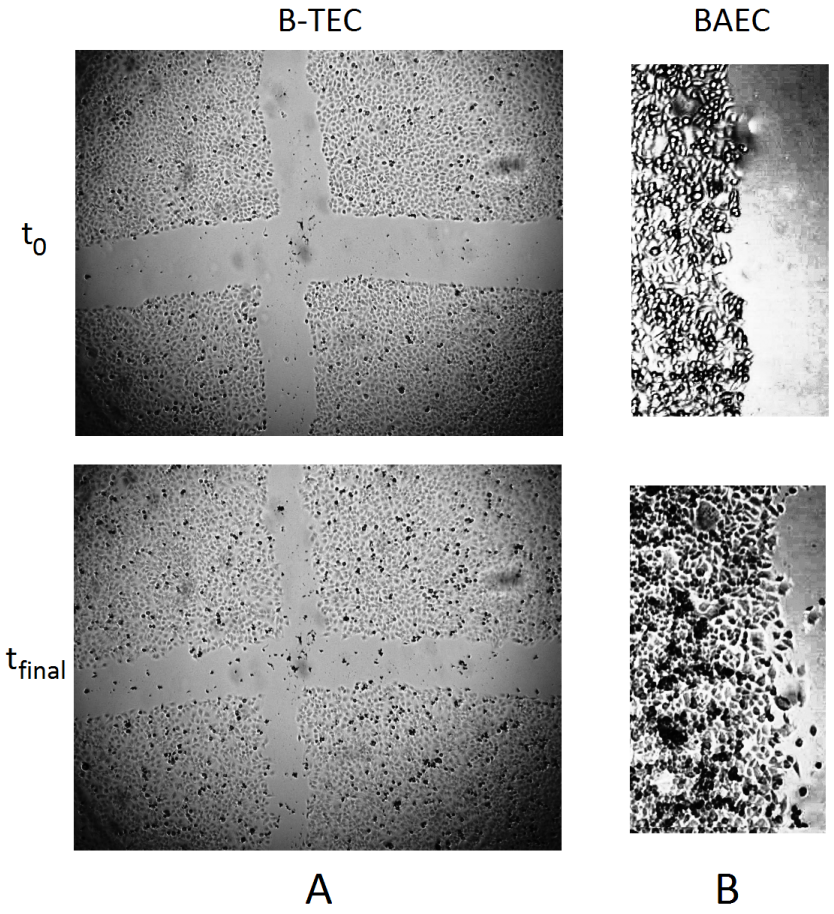

Figure 1: Different examples of wound healing assays. (A) Culture of breast tumor-derived endothelial cells (B-TEC) stimulated by 10 μM of sodium hydrosulphide (NaHS), representative images taken at $t_0 = 0$ h and $t_{final} = 8$ h after scraping. Unpublished picture, courtesy of the Cellular and Molecular Angiogenesis Laboratory of the Department of Life Sciences and Systems Biology at the University of Turin, Italy. (B) Culture of bovine aortic endothelial cells (BAEC) stimulated by hepatocyte growth factor (HGF), representative images taken at $t_0 = 1$ h and $t_{final} = 9$ h after scraping. Unpublished picture, courtesy of the Institute for Cancer Research and Treatment, Candiolo (To), Italy.

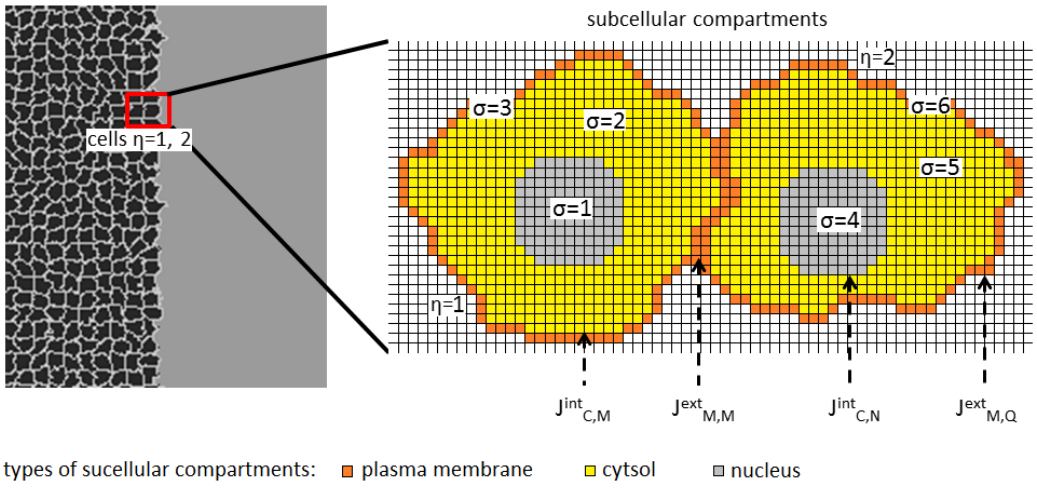

Figure 2: Representation of a pair of interacting compartmentalized cells, i.e., $\eta = 1, 2$ and of their subcellular compartments. In particular, $\sigma = 1, 2, 3$ form individual $\eta = 1$, while $\sigma = 4, 5, 6$ form individual $\eta = 2$. Lattice sites of the nuclear regions, $\tau = N$, are in grey, lattice sites of the cytosols, $\tau = C$, in yellow, and lattice sites of the plasma membranes, $\tau = M$, in orange. White sites represent instead areas of the undifferentiated extracellular medium. Black-dashed arrows indicate contact borders between subcellular compartments either belonging to the same cells, i.e., where internal adhesion energies apply, or belonging to different cells, i.e., where external adhesion energies apply.

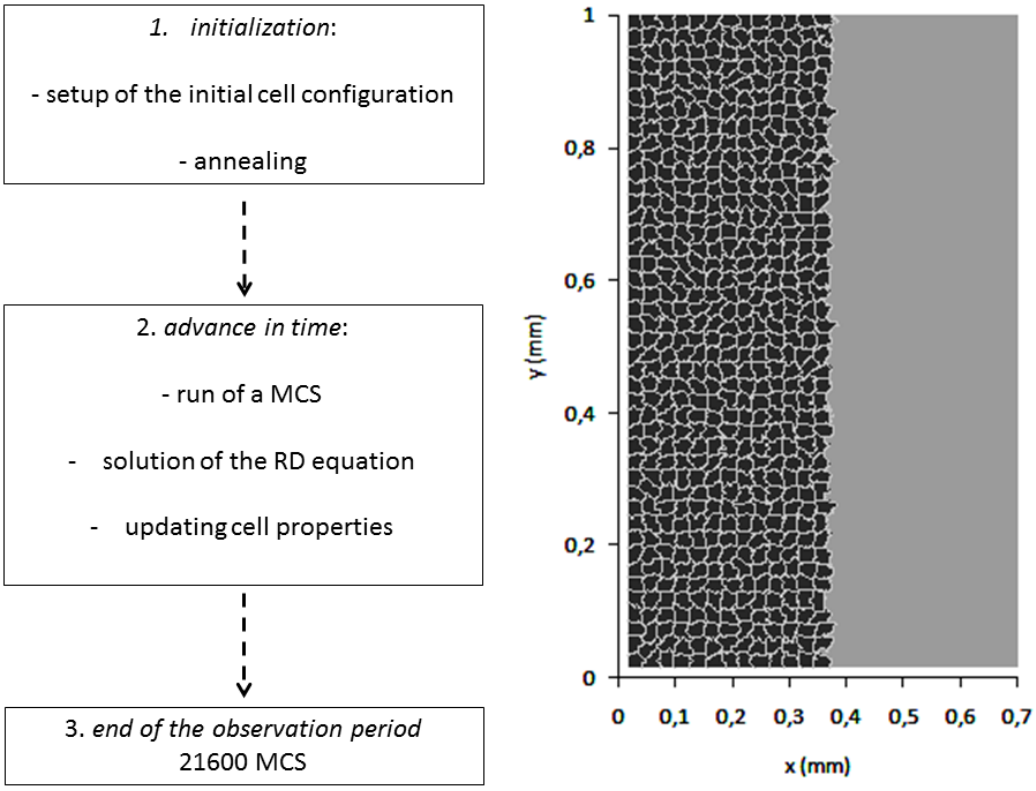

Figure 3: Left panel: conceptual scheme of the numerical algorithm underlying the proposed simulations. Right panel: initial condition (i.e., at $t = 0$) of the cell mass for all simulation settings. In this representative image, the substrate is only formed by a gelatinous homogenous medium.

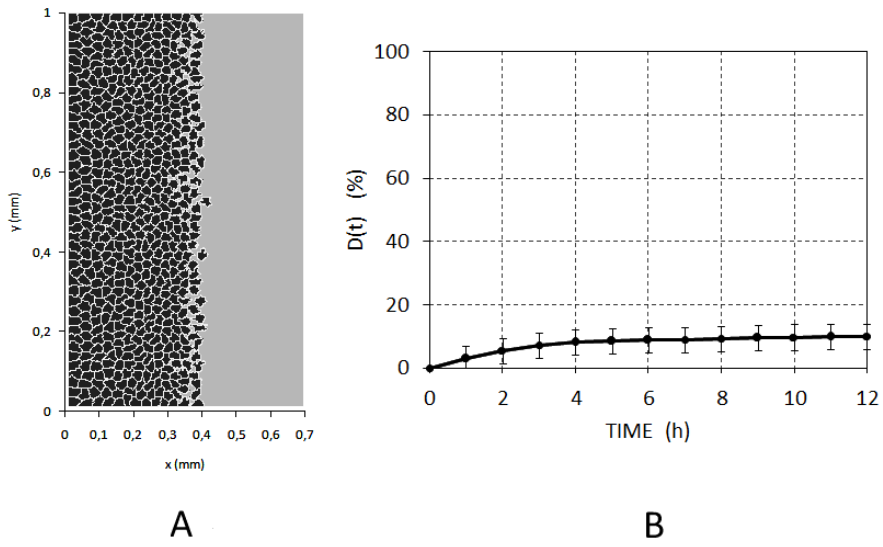

Figure 4: Healing process of the non-stimulated cellular culture. (A) Final pattern configuration (i.e., at $t = 12$ h). (B) Time evolution of the percentage of recolonized wound $D(t)$, defined in Materials and Methods.

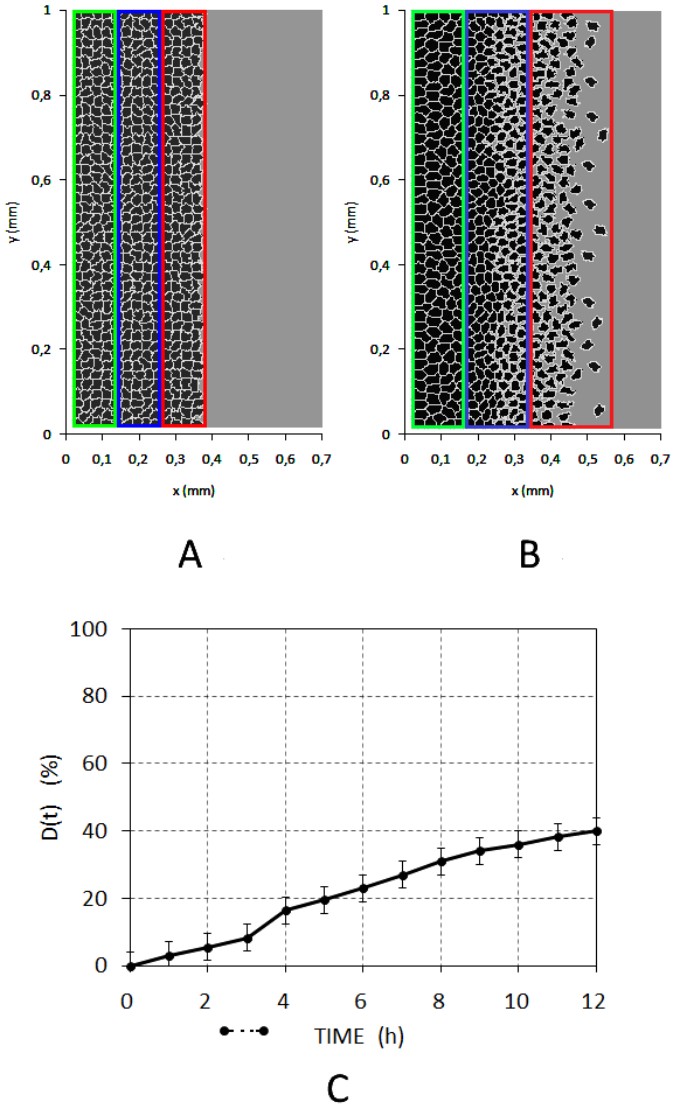

Figure 5: (A-B) Healing process of the chemically stimulated cell culture. Representative images at $t = 0$ h and $t = 12$ h, respectively. The color-coded rectangles delimit the subpopulations in which the cell culture is divided from its front, i.e., red-external, blue-middle, and green-internal. (C) Time evolution of the percentage of recolonized wound $D(t)$. The dashed segment below the graph indicates when the chemical substance is virtually added to the culture.

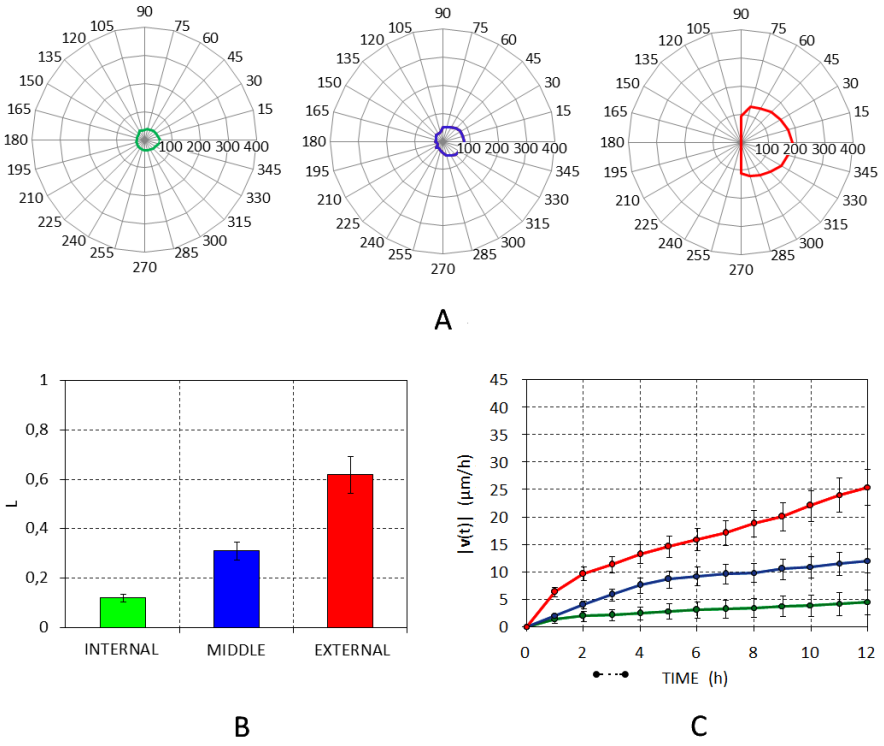

Figure 6: Migratory determinants of the three subpopulations in the case of a chemically stimulated cell culture. (A) Final displacements (in polar coordinate); (B) linearity and (C) time evolution of the modulus of instantaneous velocity. The dashed segment below the graph indicates when the chemical substance is added to the culture.

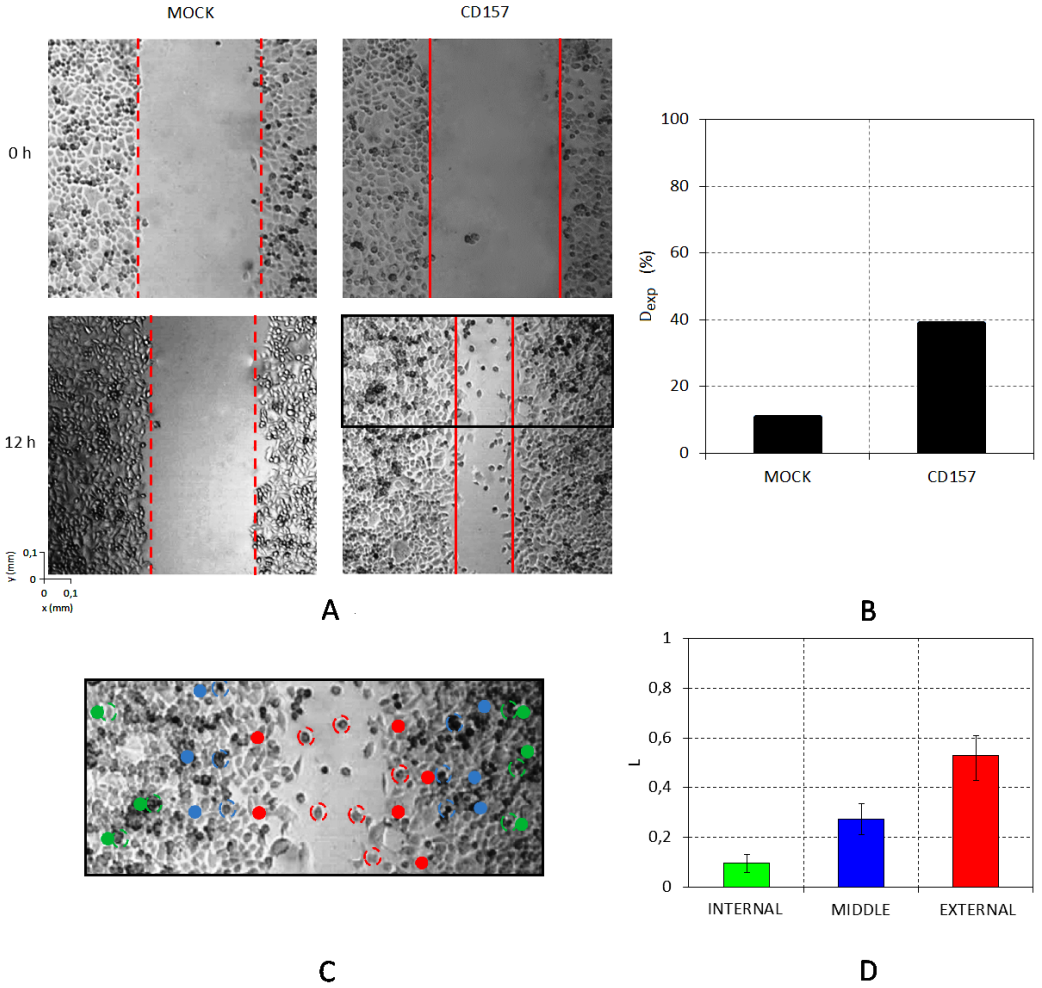

Figure 7: Experimental wound healing assay. (A-B) Graphical and quantitative evaluation of the advancement of cell population edges in the case of CD157 treatment (CD157 condition) or not (MOCK condition). (C-D) Comparison of the dynamics of representative cells initially located at different distances from the wound edges. In particular, in panel (C), the full circles indicate the initial location of the cells, whereas the dashed circumferences their final position, i.e., at 12 hours. The distinct colors are the same as those used for the analysis of the virtual wound healing, refer to Figs. 5 and 6.

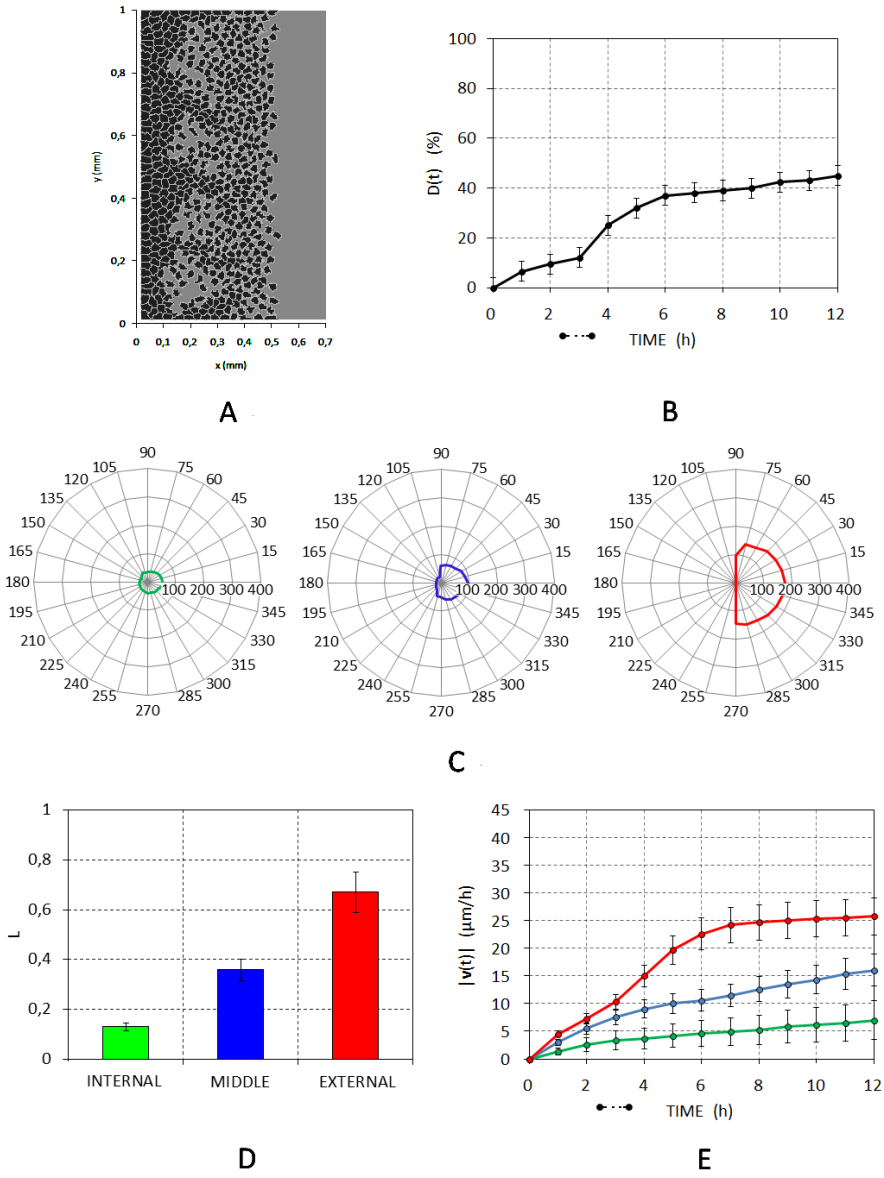

Figure 8: Wound healing process in the case of a chemically induced downregulation of cell-cell adhesion (see Eq. (8)). (A) Final pattern configuration (i.e., at $t = 12$ h). (B) Time evolution of $D(t)$. (C-D-E) Migratory determinants of the three subpopulations. The dashed segment below the graphs indicates when the chemical substance is virtually added to the culture.

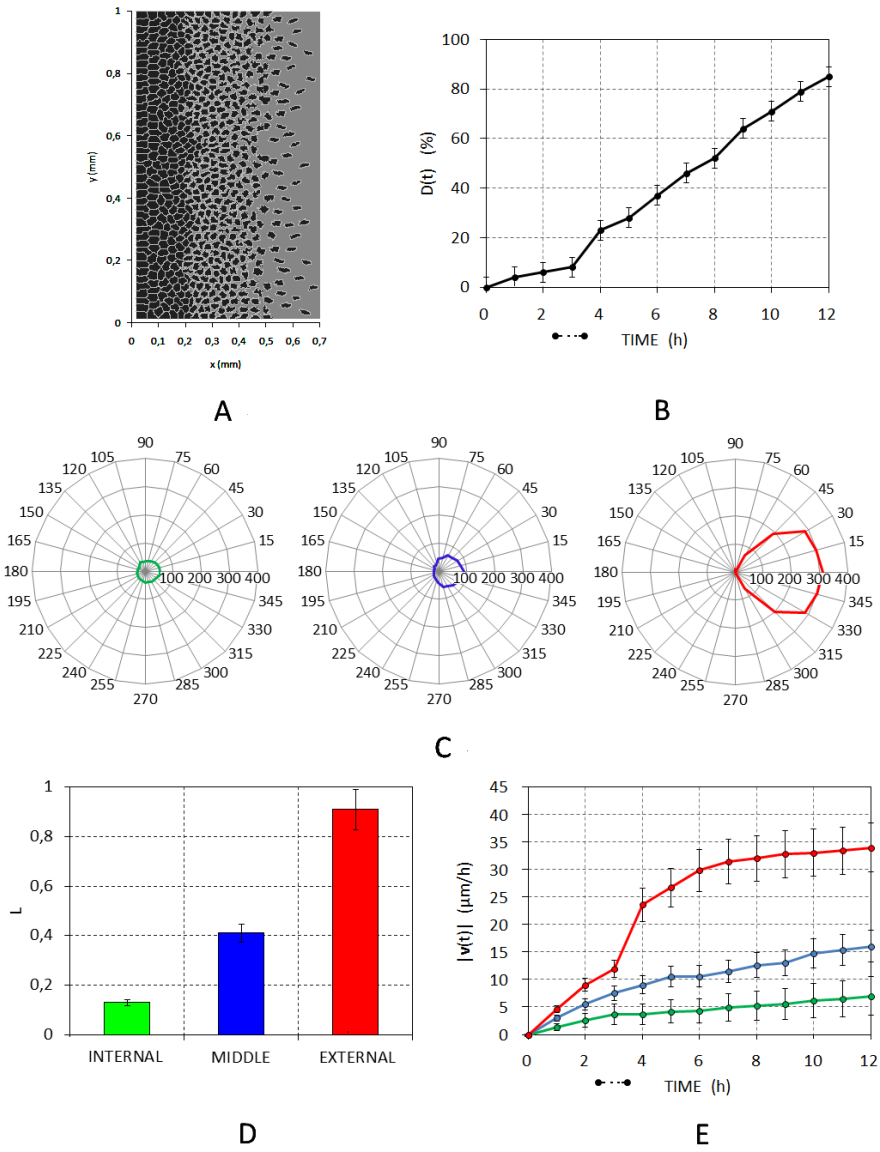

Figure 9: Wound healing process in the case of a chemically induced cell shape remodeling (see Eq. (9)). (A) Final pattern configuration (i.e., at $t = 12$ h). (B) Time evolution of $D(t)$. (C-D-E) Migratory determinants of the three subpopulations. The dashed segment below the graphs indicates when the chemical substance is virtually added to the culture.

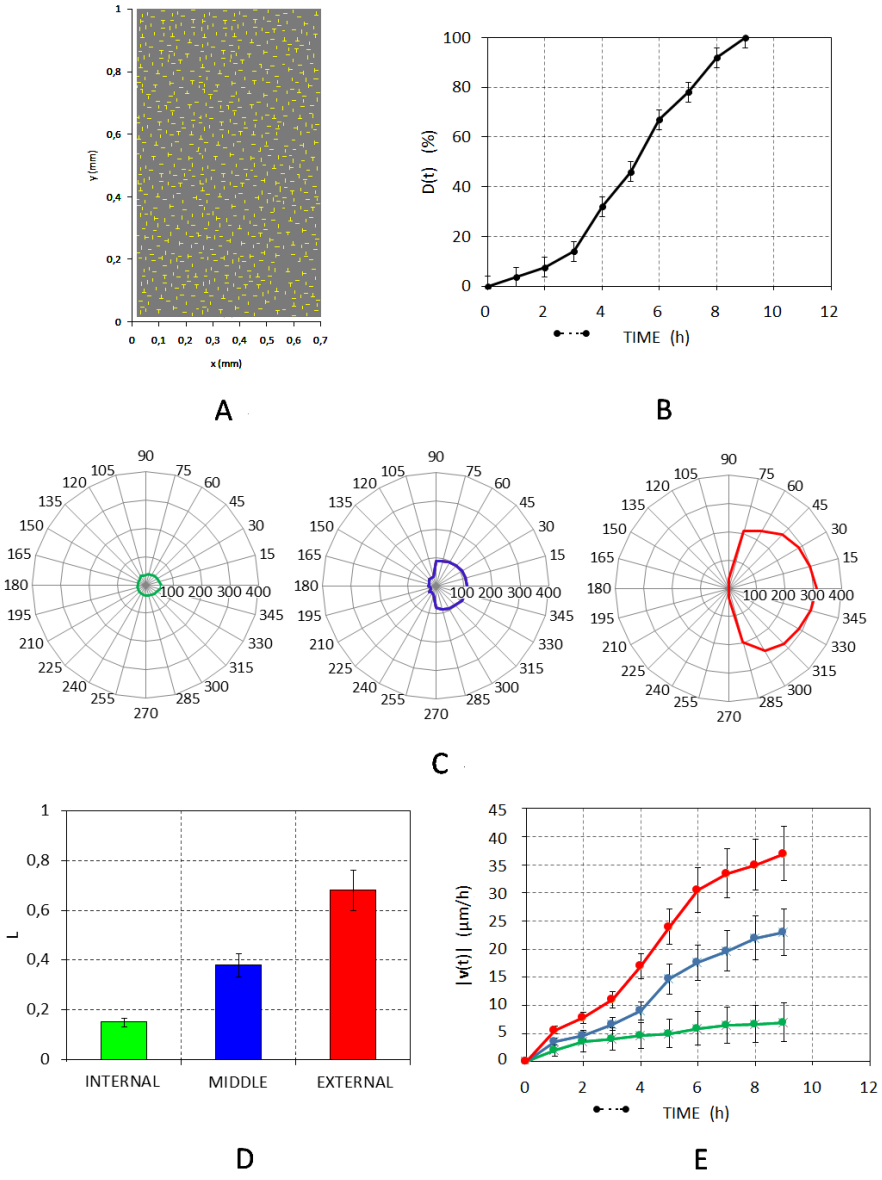

Figure 10: Wound healing process in the case of a two-component substrate. (A) Topology of the matrix. (B) Time evolution of $D(t)$. (C-D-E) Migratory determinants of the three subpopulations. The dashed segment below the graphs indicates when the chemical substance is virtually added to the culture.

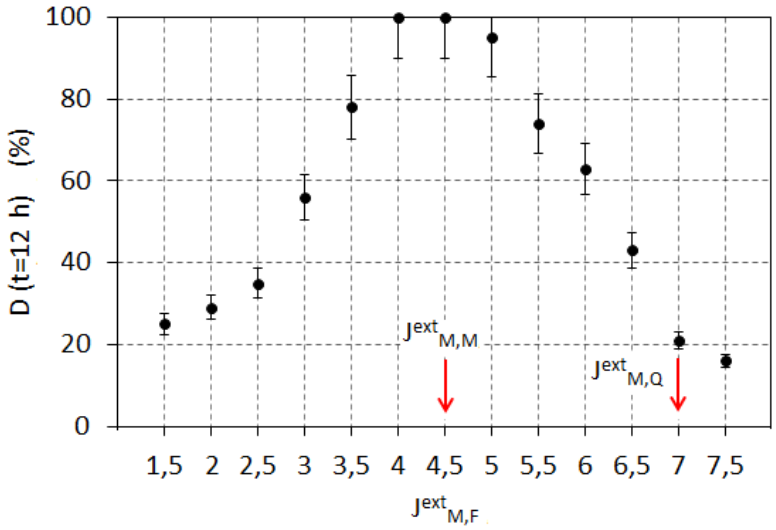

Figure 11: Effect on the healing process of variations in the cell-fiber adhesiveness, given by $J^{ext}_{M,F}$. For the readers' convenience, the value of both cell-cell adhesion, $J^{ext}_{M,M}$, and of cell-medium adhesion, $J^{ext}_{M,Q}$, are indicated in the plot.

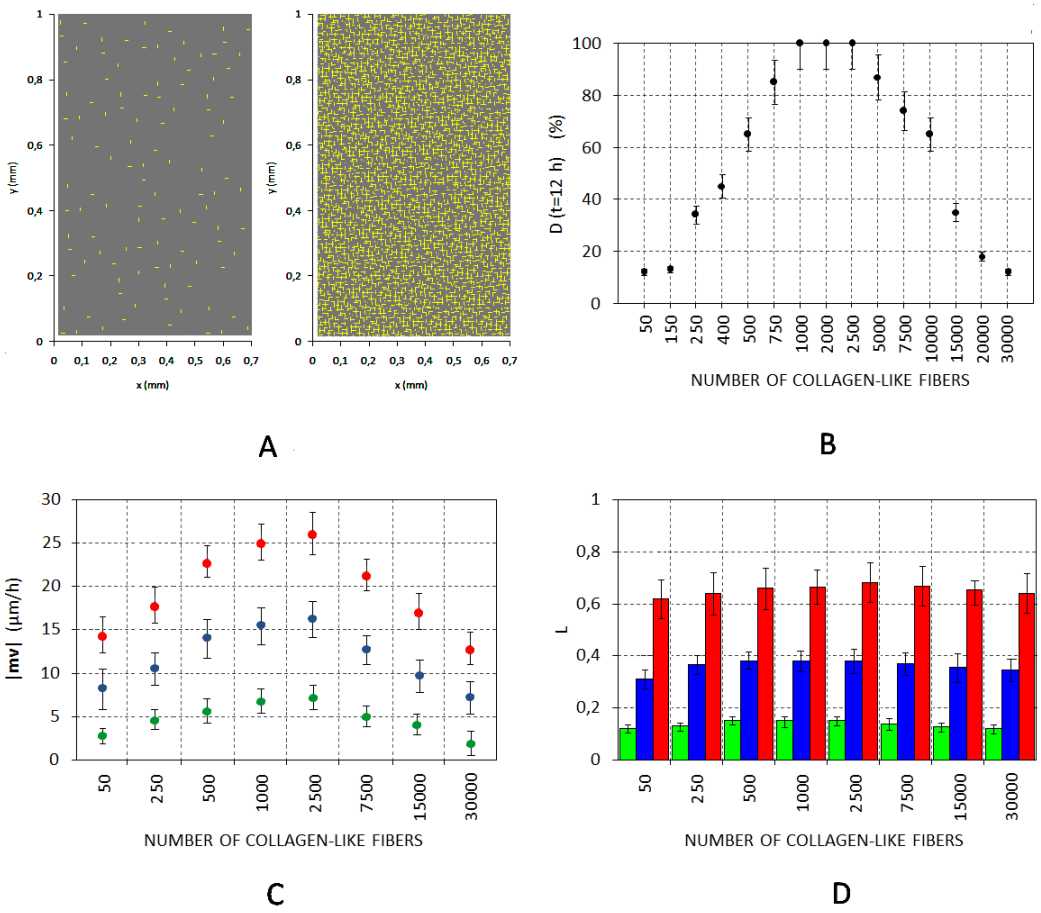

Figure 12: Healing process of the cell population seeded on substrates formed by an increasing number of fibers. (A) For representative purposes, matrices with either 150 or 15000 fibers. (B) Percentage of wound closure at $t = 12$ h vs. number of fibers. (C) Mean velocity and (D) linearity of the different subpopulations as a function of the number of fibers.

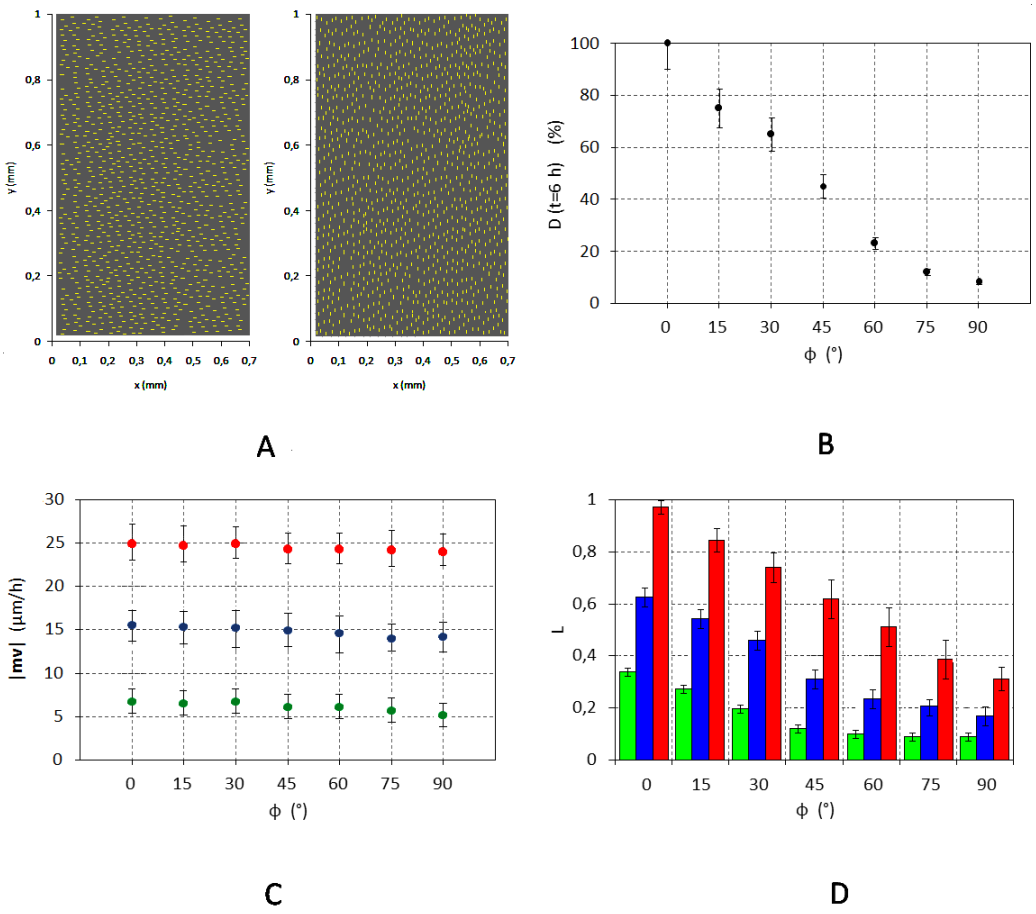

Figure 13: Healing process of the cell population seeded on substrates formed by fibers aligned in different directions. (A) For representative purposes, matrices with collagenous components disposed either along the x- or along the y-direction. (B) Percentage of wound closure at $t = 6$ h vs. fiber direction. (C) Mean velocity and (D) linearity of the different subpopulations as a function of the fiber alignment.

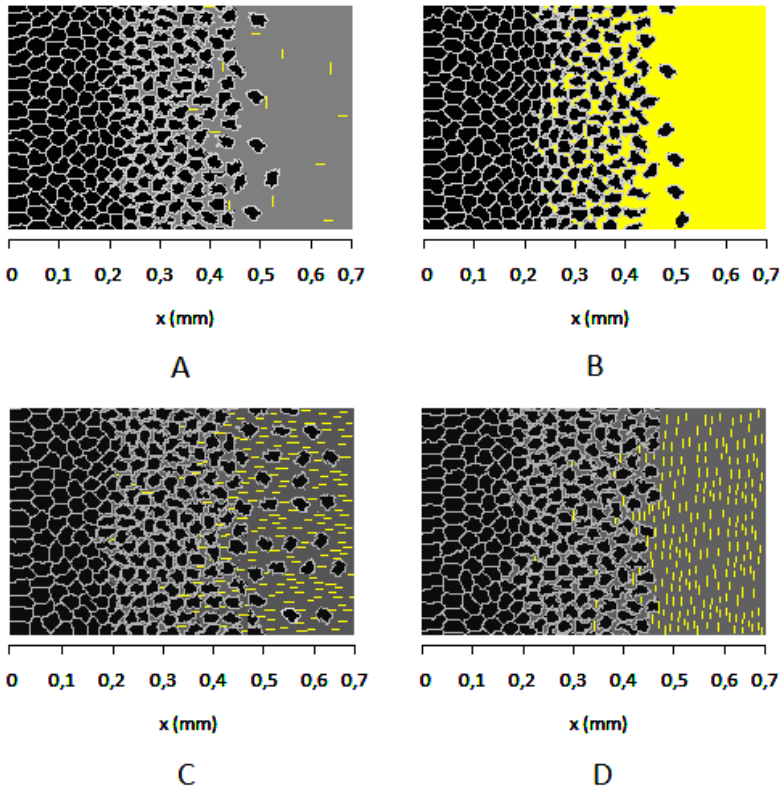

Figure 14: Representative zoom images showing details of the healing process for different two-component substrates. Matrix formed by (A) a mesh of 150 unpercolated fibers (image taken at $t = 12$ h), (B) a continuous carpet of threads (image taken at $t = 12$ h), (C) 1600 fibers aligned along the x-direction (image taken at $t = 6$ h), and (D) 1600 fibers aligned along the y-direction (image taken at $t = 12$ h).

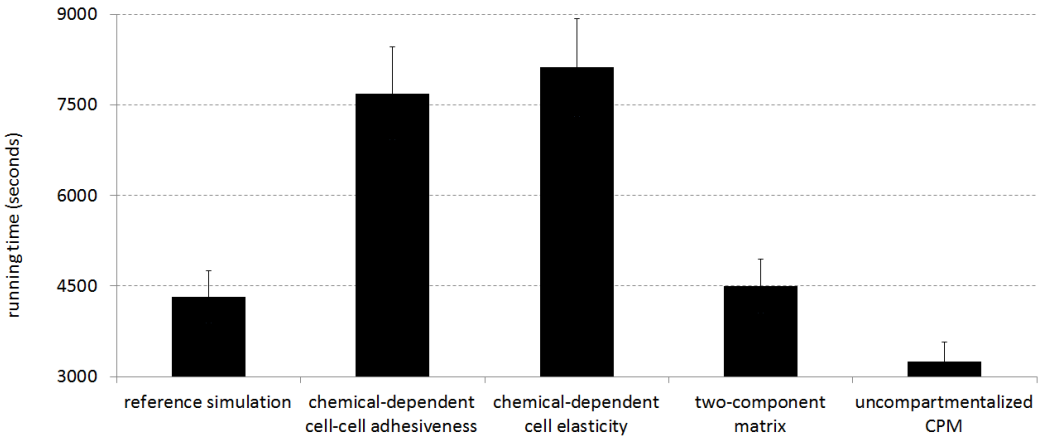

Figure 15: Running time for selected representative simulation settings. The last value refers to a wound healing process of a culture of uncompartmentalized cells in reference conditions. Values are given as mean ± SD over 100 independent simulations.

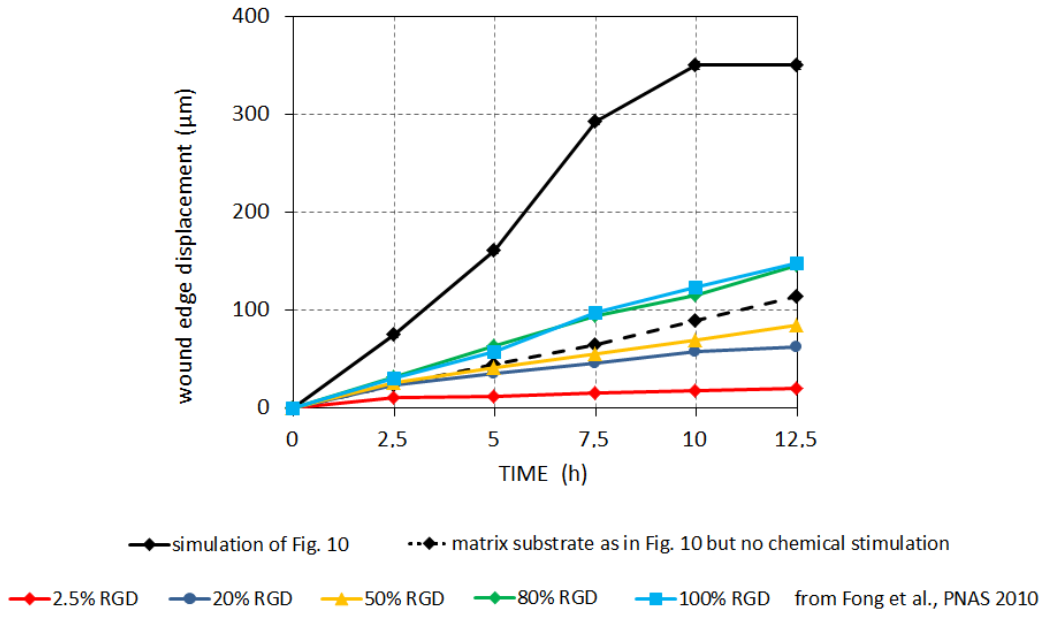

Figure 16: Wound edge displacement obtained from Fong and co-workers [44] and from selected CPM simulation settings.

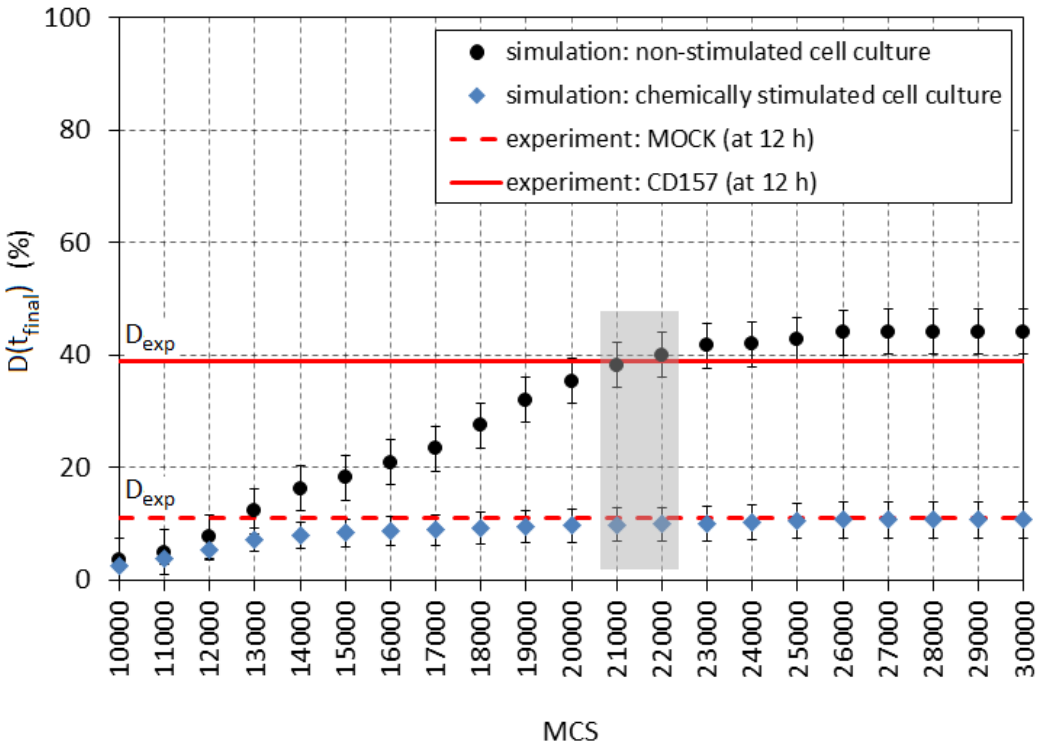

Figure 17: Percentage of recolonized wound obtained from CPM simulations for different final observation times (i.e., $D(t_{final})$) in the case of chemically stimulated or not cell culture. Red lines indicate the percentage of recolonized wound at 12 hours (i.e., D_{exp}) obtained from the assays by Ortolan et al. in the corresponding experimental conditions, CD157 or MOCK, respectively. From this plot it is possible to observe that 12 hours of actual unit of time correspond to 21600 MCS and therefore 1 MCS $\approx$ 2 seconds.